A review of nanodiamond-based photocatalysts for solar energy conversion

Zhang Wan[1,†], Cheng Xiangxiang[1,†], Guo Kesheng[2,†], Zhang Hansong[1], Li Lanxiao[3], Zhao Yongbing[4,*], Zhu Jiaqi[5,*], Wang Yongjie[1,5,*]

(1. *Guangdong Provincial Key Laboratory of Semiconductor Optoelectronic Materials and Intelligent Photonic Systems*, *Harbin Institute of Technology*, *Shenzhen* 518055, *China*;
2. *Ji Hua Laboratory*, *Foshan* 528200, *China*;
3. *Department of Materials Science and Engineering*, *National University of Singapore*, *Singapore* 117579, *Singapore*;
4. *School of Physics and Electronics*, *Yancheng Teachers University*, *Yancheng* 224007, *China*;
5. *National Key Laboratory of Science and Technology on Advanced Composites in Special Environments*, *Harbin Institute of Technology*, *Harbin* 150080, *China*)

Abstract: Photocatalysis is an important technology for using solar energy to produce hydrogen, convert CO_2 to synthetic fuels, and decrease persistent pollutant. However, conventional photocatalysts have limitations, including poor spectral absorption, inefficient charge separation, and structural instability under operational stress, which demand innovative durable materials with tailored electronic properties. Nanodiamond (ND) has recently been recognized as a suitable material because of its exceptional chemical stability, superior charge carrier mobility, and possible surface functionalization. While its intrinsic wide bandgap limits its response to visible-light, different methods have been demonstrated to activate its catalytic potential. Here, several emerging strategies for improving the catalytic performance of ND-based photocatalytic systems are summarized, including surface functionalization, plasmonic hybridization, heteroatom doping, and heterostructure design. And the structure-activity relationship and design principle are proposed to improve the light harvesting, charge transport, and redox kinetics for constructing high efficiency ND-based photocatalysts used in the renewable energy and environmental industries.

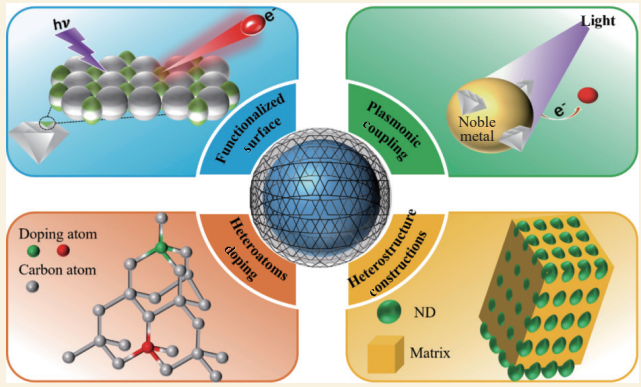

Key words: Photocatalysis；Nanodiamond；Solar fuel conversions；Functionalization；Doping；Heterostructure

1 Introduction

The direct and effective utilization of solar energy has become a key component of sustainable fields, such as photocatalysis, thermal catalysis, photovoltaic and photothermal power generation[1–3]. Photocatalysis, which mimics natural photosynthesis by leveraging semiconductors to drive redox reactions under light irradiation, has emerged as a cornerstone technology for solar energy cycles[4–8]. Its applications span 3 critical domains: (1) solar water splitting for hydrogen production[9–13]; (2) CO_2 photoreduction to value-added hydrocarbons[14–18]; (3) environmental remediation via radical-mediated pollutant degradation[19–21]. The International Energy Agency asserts that hydrogen and hydrogen-based fuels play a pivotal role in achieving net-zero emissions.

Unfortunately, traditional semiconductor photocatalysts face multiple key challenges due to their

Received: May 22, 2025
Revised: July 20, 2025
Accepted: July 21, 2025

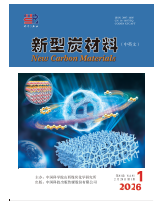

inherent limitations in practical applications. Most photocatalysts possess wide band gap (E_g), rendering them capable of excitation solely by ultraviolet (UV) or near UV light. For example, ZnO (3.3 eV) and TiO_2 (3.2 eV) have wide bandgaps, and can utilize only 4% of the solar energy in the UV[22–23]. While doping (e.g., N, S) or defect engineering can extend the absorption edge into the visible region[24], such modifications frequently result in an augmentation of carrier recombination centers, consequently diminishing quantum efficiency. Furthermore, the energy conversion efficiency is severely constrained by inadequate charge separation, electron–hole recombination and slow transport, as well as sluggish interfacial reactions. Meanwhile, concerns regarding thermal, hydrothermal, and chemical stability have the potential to jeopardize the photocatalytic lifetime, a predicament in practical applications. Additionally, the presence of toxic deactivation in photocatalysts represents a critical defect in photocatalytic applications[25]. These limitations necessitate advanced materials with broad light absorption, efficient charge separation, and robust stability.

Nanodiamond (ND) has arisen as a revolutionary catalytic platform, uniquely positioned to overcome conventional semiconductor limitations through distinguished structural and electronic properties[26]. As prototypical zero-dimensional carbon nanomaterials (diameter of 1–100 nm), NDs feature a sp^3-hybridized tetrahedral lattice that confers remarkable core characteristics[27]. The diamond matrix exhibits exceptional chemical resilience, maintaining structural integrity under extreme acidic/alkaline conditions and prolonged exposure to reactive oxygen species, a critical advantage for sustained photocatalytic operation in harsh environments[28–29]. Surface engineering flexibility represents another key attribute, including establishment of homogeneous initial surface termination (e.g., —COOH, —OH, —H, $—NH_2$), covalent and non-covalent immobilization of diverse functional groups (e.g., enzymes, halogens), and subsequent grafting of larger (bio)molecules[30–31]. Notably, NDs exhibit intrinsic biocompatibility and are free of toxic heavy metals (e.g., Cd, Pb), rendering them uniquely advantageous for biomedical photocatalytic applications such as antimicrobial surface engineering and photodynamic cancer therapy[32]. Their exceptional thermal conductivity (~ 2200 $W \cdot m^{-1} \cdot K^{-1}$) surpasses that of conventional semiconductors by orders of magnitude, effectively dissipating localized thermal stresses during photocatalytic operation and thereby preventing structural degradation[33]. Furthermore, their high charge-carrier mobility (~ 4500 $cm^2 \cdot V^{-1} \cdot s^{-1}$) facilitates rapid separation and transport of photogenerated charges to reactive sites, significantly reducing electron–hole recombination losses[34–35].

The application of NDs in photocatalysis has demonstrated remarkable performance across a broad spectrum of reactions, including ambient-condition nitrogen fixation, selective CO_2 conversion, solar hydrogen evolution, and pollutant degradation. A pivotal breakthrough was achieved in 2013 when Hamers et al.[36] discovered that hydrogen-terminated diamond surfaces could inject photoexcited electrons into aqueous media, enabling the reduction of N_2 to NH_3 at ambient temperature and pressure under UV illumination. This discovery established a new paradigm for photocatalytic reduction, whereby electrons are directly delivered to reactants without the need for molecular adsorption on the surface. Subsequently, the versatility of NDs in CO_2 coversion to fuels was futher revealed. The one-electron reduction pathway of CO_2 ($CO_2 + e^- \rightarrow CO_2^-$) was realized through UV excitation of diamond substrates, followed by direct injection of electrons into water to form solvated electrons, ultimately producing CO with >90% selectivity[37]. This method avoided the limitation of traditional electrochemical or photochemical processes where CO_2 needed to be adsorbed on the surface, and provided a new pathway for CO_2 reduction.

To enhance ND-based photocatalysis, advanced heterostructures have been rationally engineered through deliberate material hybridization. For instance, Su et al.[38] fabricated ND@g-C_3N_4 heterostructures by pyrolysis, achieving a significant im-

provement in H_2 evolution rates (59.1 μmol·h^{-1}) compared with pristine g-C_3N_4 (10.5 μmol·h^{-1}) under visible-light irradiation. The incorporation of NDs effectively enhanced light scattering, extended visible-light absorption, and facilitated photogenerated charge separation within the heterostructure. In the field of environmental remediation, NDs have also shown great potential as adsorbents and ion exchangers for the efficient removal of toxic heavy metal ions and organic dyes from water, owing to their abundant polar surface functional groups[39–40]. For instance, g-C_3N_4@ND nanocomposites synthesized by hydrothermal treatment exhibited enhanced photocatalytic degradation of Rhodamine B under visible light. This improvement was attributed to the strong interfacial interaction between g-C_3N_4 and ND, which suppressed electron–hole recombination and promoted charge-separation efficiency[41]. Recently, numerous reviews have comprehensively summarized the properties of diamond and its catalytic applications in hydrogen evolution, oxygen reduction, and carbon dioxide reduction reactions, along with wastewater treatment[5,32,42–44]. However, systematic discussions on strategies to enhance the catalytic efficacy of ND-based materials remain limited, particularly with respect to underlying mechanistic insights. This review aims to fill this gap by highlighting recent advances in ND-based photocatalysis from the perspective of material modification strategies.

Despite the noteworthy advancements in the realm of photocatalysis, the activity of pristine or untreated NDs is weak because of charge carrier recombination, narrow light absorption range and slow charge transfer. The high aggregation ability and poor water dispersibility also restrict their practical applications in wastewater treatment[42]. Hence, modification strategies are imperative to enhance the photocatalytic activity of ND-based systems. Here, this review concisely summarizes the preparation methods of NDs, followed by the comprehensive and predominant modification strategies to ameliorate the catalytic activity. Specifically, the alterations include following: (1) surface functionalization, tailoring termination groups (e.g., —H, —NH_2) to modulate electron injection barriers and interfacial reactivity; (2) heteroatoms doping, implementing element doping (e.g., B, N) to narrow the bandgap and create mid-gap states; (3) heterojunction construction, such as ND@g-C_3N_4, ND@TiO_2, to spatially separate photogenerated carriers; and (4) plasmonic hybridization, integrating noble metal nanostructures (e.g., Au, Ag) to leverage localized surface plasmon resonance effects for visible-light sensitization, as summarized in Fig. 1. Finally, a summary of the performance advantages of ND-based photocatalysts is provided, along with indications of future research directions, includ-

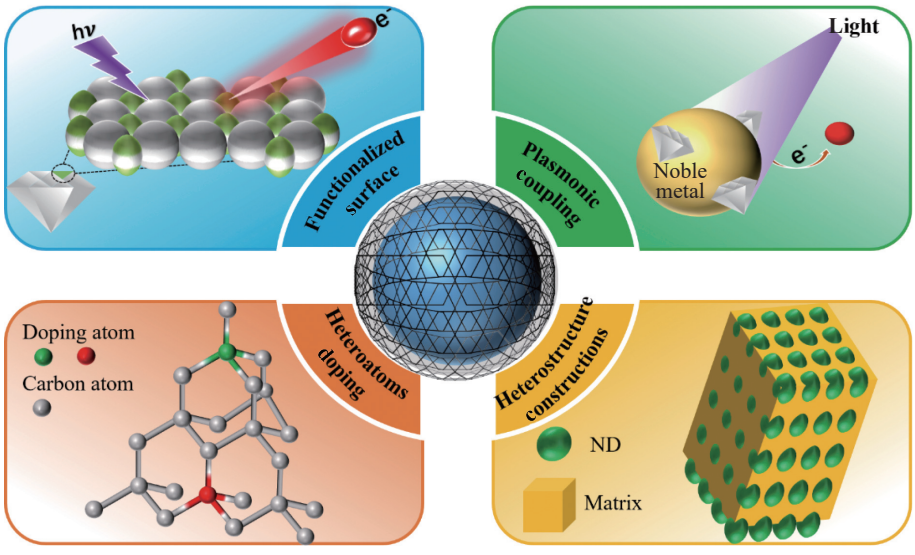

Fig. 1 An overview of modification strategies for ND-based photocatalysts

ing scale-up ND preparation, further development of photocatalytic mechanism, and directions prioritized of photocatalytic application.

2 Preparations of NDs

NDs have emerged as promising photocatalysts owing to their tunable electronic properties and exceptional stability. However, their photocatalytic efficiency is intrinsically determined by the synthesis methods, which govern structural features such as crystallinity, surface chemistry, defect density, and particle size distribution. This section reviews the main synthesis techniques, highlighting their underlying mechanisms and the resulting implications for the structural characteristics of NDs.

2.1 Detonation synthesis

The detonation method[45], developed by Soviet scientists in the 1960s as a means to synthesize diamonds, involves the use of explosives within a closed chamber to generate shock waves. These shock waves, in conjunction with the high temperatures and pressures present, facilitate the conversion of carbon into diamonds[46–47]. This way is based on the phase transition of graphite, utilizing explosives such as TNT or hexogen to generate extreme temperatures and pressures. Alternatively, the method might be based on the phase transition of carbon precursors, employing mixtures such as RDX/carbon black, RDX/graphite and gunpowder/RDX/graphite[48].

Detonation nanodiamonds (DNDs) possess a core-shell structure, with a 3–5 nm sp^3 hybridized carbon core surrounded by a shell composed of a mixture of sp^2 and sp^3 carbon along with oxygen-containing functional groups. Due to the explosive detonation synthesis, the surfaces of DNDs are typically heterogeneous. These heterogeneities include nonpolar fullerene-like reconstructions, negatively charged polar groups such as carboxylic acid and anhydrides, and positively charged polar portions including hydroxyls, hydrogens, and amino functionalities[49–50]. Fig. 2a illustrates the key structural features of detonation soot and the purified DND product. The non-diamond carbon components have been found to contain graphite nanocrystals, carbon onions, and other amorphous carbon. They are located on the exterior of compact DND aggregates, and can be removed during the purification process. Alternatively, they may be confined to compact aggregates, remaining inaccessible to the oxidizing medium[51].

Owing to sp^2 carbon shell, DND band gaps are in

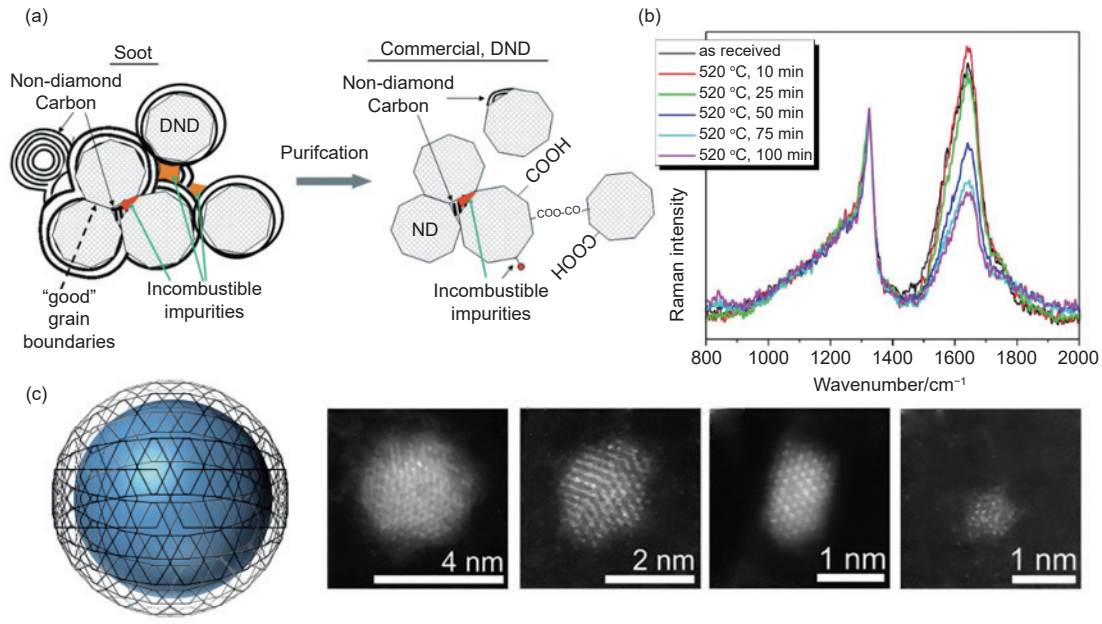

Fig. 2 (a) Scheme of structural components of detonation soot and DND product[51]. Copyright © 2009, Taylor & Francis. (b) Raman spectra of the size reduced DNDs[54]. (c) The core-shell structure and STEM images of different size reduced DNDs[54]. Copyright © 2016, Springer Nature

the range of 2–3.5 eV, which is much narrower than the value for single-crystal diamond[52]. The dimensions of diamond microcrystals are determined by the brief duration of the explosion[53]. Stehlik et al.[54] used air anneal under specific conditions to reduce average DND particle sizes to below 2 nm. The Raman spectroscopy (Fig. 2b) provided average results of microscopic structural details on single particle level. An amorphous sp^3 phase (the peak at ~ 1324 cm^{-1}) was persistent during the annealing process, and the 1500–1800 cm^{-1} band originated from surface or near-surface sp^2 carbon atoms. Representative STEM images of the annealed DNDs (520 °C, 25 min) were shown in Fig. 2c, presenting not only the perfectly crystalline DNDs but also some number of partially disordered DNDs with crystalline domains. This structural duality, where ordered crystalline cores coexist with disordered surface phases, enables tunable electronic properties unattainable in bulk diamond. In general, detonation enables cost-effective mass production of core-shell structured NDs with versatile surface functionalization, while it suffers from persistent metallic impurities and requires aggressive post-processing to remove graphitic byproducts.

2.2 Chemical vapor deposition (CVD)

The scientific exploration of CVD diamond synthesis originated through seminal independent investigations by Angus (USA)[55] and Derjaguin (USSR)[56] during the early 1968s. Building upon the foundational discoveries, a Japanese group led by Setaka subsequently systematized CVD methodologies through plasma generation mechanism, while pioneering key technological variants including hot filament, radio-frequency plasma and microwave plasma CVD[57]. This advanced synthesis technique operates through sequential physicochemical processes: precursor gas dissociation into reactive hydrocarbon radicals under non-equilibrium thermodynamic conditions, followed by surface diffusion and adsorption of these species onto substrates (Fig. 3a). The fundamental gas mixture generally consists of methane as the primary carbon feedstock, and hydrogen fulfilling dual catalytic

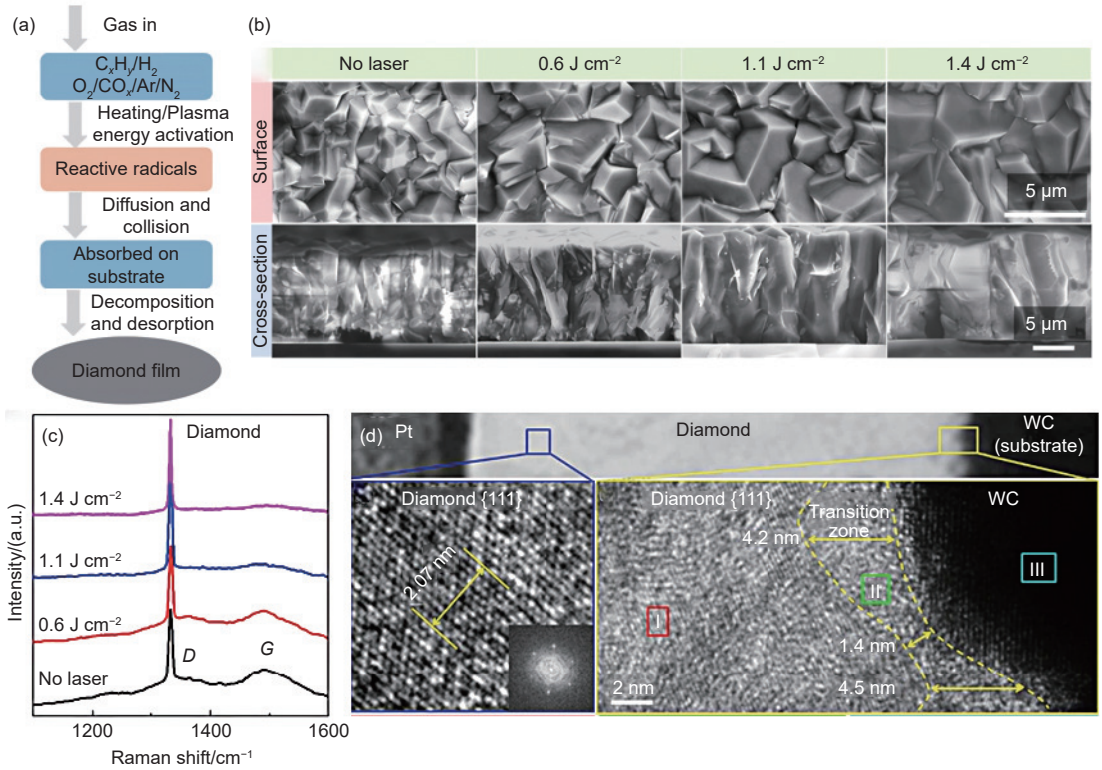

Fig. 3 (a) Flow chart of CVD diamond preparation process[60]. (b) SEM images of surface and cross-sectional morphologies of diamond films. (c) Raman spectra of corresponding diamond films. (d) TEM images of a 389 nm thick diamond film on a substrate prepared with UV laser irradiation at 1.4 J·cm^{-2}[61].

functions. The hydrogen contributes to the generation of methyl radicals, while concurrently etching graphitic carbon impurities through selective oxidation. Thermal decomposition of hydrocarbons at elevated temperatures generates atomic carbon intermediates that undergo catalyst-mediated reconstruction into sp^3-hybridized diamond nuclei[58].

The growth architecture demonstrates remarkable tunability, where substrate engineering (surface pretreatment, crystalline orientation), process parameters (pressure, temperature gradients), and auxiliary gas additives (nitrogen, oxygen) collectively dictate nucleation density, crystallographic orientation, and surface termination chemistry[59–60]. For instance, UV laser photolysis of hydrocarbon species within a combustion flame significantly enhanced diamond growth and quality. This process has increased the growth rate of diamond by more than doubled and improved diamond quality by 4.2%. Crucially, UV laser irradiation in a parallel-to-substrate geometry shortened diamond nucleation time and suppressed non-diamond carbon accumulation. Grain growth analysis revealed laser fluence-dependent enlargement and homogenization of diamond crystallites (Fig. 3b). Raman spectroscopy confirmed higher diamond quality and purity with UV irradiation, evidenced by a sharper and more intense diamond peak (1332 cm^{-1}) and reduced *D*/*G* bands (1370, 1500 cm^{-1}) representing impurities (Fig. 3c). TEM imaging (Fig. 3d) further verified the excellent crystalline structure of the UV-grown diamond films[61]. This multi-parameter control paradigm enables precise engineering of diamond microstructures for advanced applications. Generally, CVD achieves exceptional phase purity and controlled crystallinity for high-quality films or discrete particles, but the process exhibits slow growth kinetics and faces significant substrate compatibility constraints.

2.3 Laser ablation

Liquid-phase laser ablation is a versatile and cost-effective approach for ND synthesis, achieved by pulsed laser irradiation of carbonaceous targets (e.g., graphite or carbon black) in liquid media[62]. This process induces rapid target disintegration through photothermal melting and vaporization, generating carbon-rich plasma plumes. The confined liquid environments promotes diamond nucleation by rapid quenching of metastable carbon clusters, while transient plasma dynamics limit particle growth. The extreme thermal gradients and quenching kinetics allow for precise size control, with laser fluence, pulse duration, and solvent selection serving as key parameters to tailor ND characteristics[63–65].

The ablation process parameters, including laser fluence, pulse duration, and solvent selection, serve as critical parameters governing particle size distribution. For instance, Hao et al.[66] utilized 343 nm femtosecond laser ablation in liquid to controllably prepare bare NDs, achieving a mean size of 3 nm. Key parameters governing the process included the laser scanning point interval (LSPI), laser energy, and liquid medium (Fig.4a, b). While laser energy minimally affected particle size, it significantly altered the intrinsic structure and sp^3/sp^2 ratio. The liquid medium critically influenced both the mean size and structural properties. Replacing water with ethanol (keeping ablation parameters unchanged) yielded NDs@ethanol (Fig. 4c) averaging 3.8 nm, compared with 3.3 nm for NDs@water (Fig. 4d), attributed to differing ablation-induced temperature and pressure. Raman spectra (Fig. 4e) showed consistent peak positions and widths for both types, but a lower relatively intensities I_D/I_G (~ 1.0) for NDs@water vs. NDs@ethanol (~ 1.5), indicating a higher relative proportion of sp^3 carbon in the ethanol-derived NDs. FTIR analysis (Fig. 4f) revealed significantly more surface oxygen-containing functional groups (e.g., C=O at 1723 cm^{-1}, C−O−C at 1113/1074 cm^{-1}) on NDs@ethanol, indicating more complex surface modification compared to NDs@water. These findings establish solvent-mediated control over diamond nucleation kinetics and surface termination. Laser ablation rapidly generates ultrasmall, well-dispersed NDs with >90% sp^3 content without surfactants, but practical adoption is hindered by low production yields and high energy consumption.

2.4 Cavitation

Cavitation-mediated synthesis has been used for

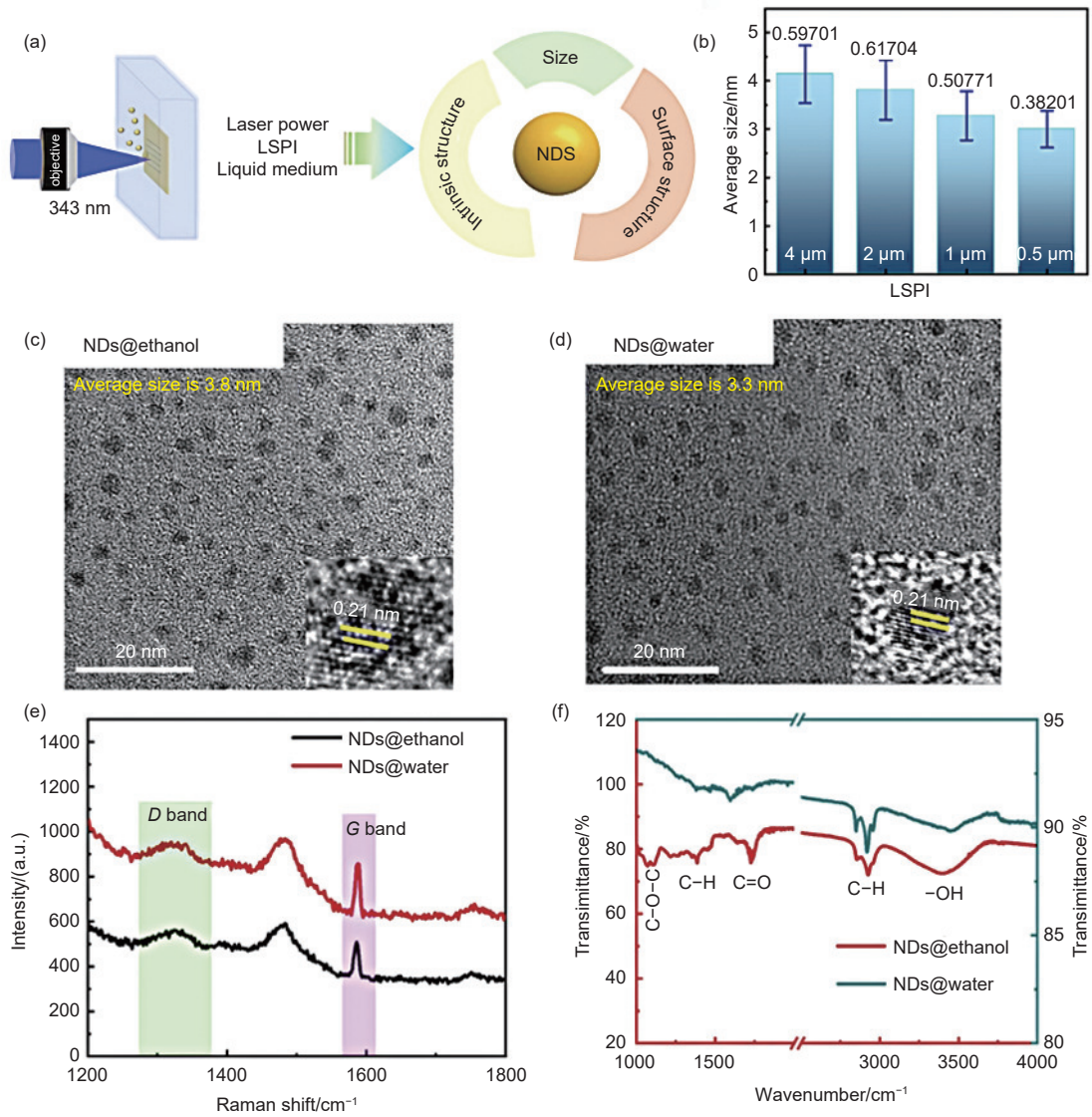

Fig. 4 (a) Controllable preparation of bare NDs through laser ablation in liquid. (b) Average size variation of NDs at different LSPI. TEM images of NDs fabricated (c) in ethanol, (d) DI water and the HRTEM displayed by the insets. (e) Raman spectra and (f) FTIR of NDs obtained in either ethanol or DI water[66].

ND fabrication, with its conceptual orgins tracing back to Galimov's pioneering hypothesis in 1973, which proposed that diamonds could form under natural fluidic conditions by cavitation-induced phase transformation[67–68]. This innovative approach capitalizes on the extreme transient thermodynamic states generated during cavitation bubble collapse within carbonaceous fluids, conditions thermodynamically favorable for metastable diamond phase stabilization. Galimov's pioneering experimental validation in 1989 demonstrated the feasibility of this mechanism using benzene as both solvent and carbon precursor, where ultrasonic cavitation generated carbon particulates containing crystalline diamond nanoparticles alongside polymeric byproducts[69]. Subsequent advancements by Voropaev et al.[70] in ethanol–aniline systems yielded monodisperse NDs (3−5 nm) with improved crystallinity, highlighting the critical role of solvent selection in controlling nucleation kinetics. The major methods for inducing cavitation include ultrasound cavitation[69], hydrodynamical cavitation[71] and laser-induced cavitation[72]. The ultrasonic synthesis mechanism involves controlled generation and implosion of micron-scale vapor cavities in graphite-dispersed liquids, creating localized transient plasma states that drive $sp^2 \rightarrow sp^3$ carbon restructuring. This

non-catalytic, ambient-pressure technique offers distinct advantages in energy efficiency and scalability though challenges remain in achieving narrow size distributions and phase purity.

2.5 Ball milling

Ball milling is a process that utilizes high-energy ball milling of natural or synthetic diamonds (e.g., CVD-synthesized diamonds) to refine them into nanoscale diamonds[73]. The resultant nanoparticles exhibit a core-shell architecture comprising a crystalline diamond core encapsulated within a structurally complex surface layer containing graphitic carbon domains and processing residues[74]. This process leverages intense mechanical forces generated through high-velocity collisions between milling media (typically hardened steel) and diamond particles, inducing progressive size reduction through fracture propagation. However, conventional ball milling produces polydisperse size distributions and heterogeneous surface chemistries, necessitating downstream purification. Eskandarany et al.[75] introduced a novel room-temperature synthesis method for ultrafine NDs embedded within an amorphous-carbon matrix, achieved by high-energy ball milling (Fig. 5a) of commercial graphite under helium atmosphere. A schematic diagram of the graphite-to-ND phase transition was proposed in Fig. 5b. The process involved distinct phase transformations: initial ball milling (0–10 h) destabilized graphite into a metastable phase of single-walled carbon nanotubes (SWCNTs). Continued milling (16 h) completely converted the SWCNTs into an amorphous-carbon phase. During the final milling stage (16–28 h), the persistent application of heavy impacts and shear forces by the milling media drived the majority of this amorphous carbon towards its most thermodynamically stable state, forming NDs. Quantitative analysis using XRD and Raman spectroscopy revealed the final product consists of approxim-

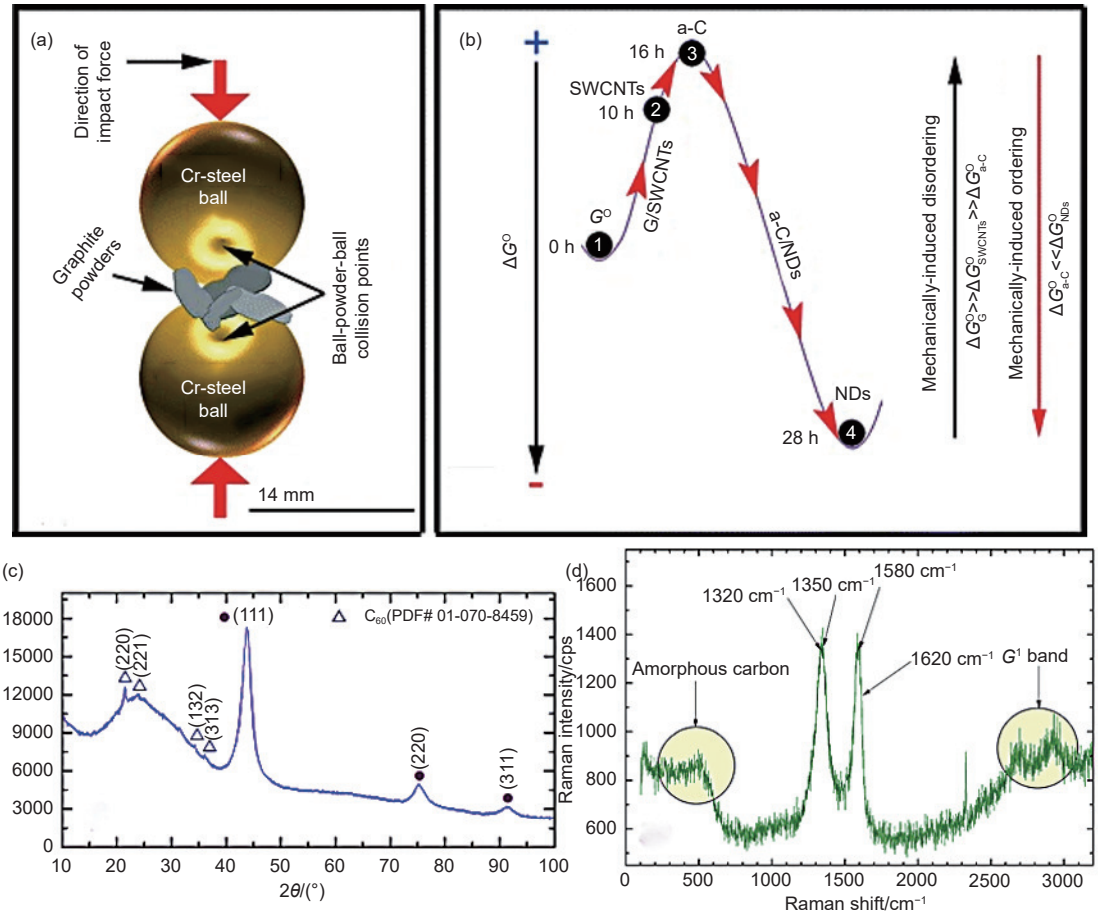

Fig. 5 (a) Ball-powder-ball collision dynamics during high-energy milling of graphite. (b) Evolution of formation free energy ($\Delta G°$) driving graphite-to-ND phase transitions across milling stages. (c) XRD pattern and (d) Raman spectrum of the final ND composite[75]. Copyright © 2017, Springer Nature

ately 81% crystalline phase (predominantly NDs along with some C_{60}) and 19% amorphous carbon. The broadening shown in the (111), (220), and (311) Bragg peaks (Fig. 5c) implied the formation of nanocrystalline diamond after ball milling. Raman spectroscopy (Fig. 5d) confirmed the transformation, showing characteristic ND peaks at ~ 1320 cm^{-1} (assigned to a slightly downshifted tetrahedral sp^3 band, indicative of lattice distortion and imperfections induced by the prolonged milling) and ~ 1620 cm^{-1} (related to sp^2 carbon). Generally, ball milling offers simple, scalable processing with adjustable particle sizes through mechanical parameters. It also introduces structural defects and yields polydisperse particles with mixed sp^2/sp^3 hybridization.

In addition to the aforementioned synthesis methods, traditional high-temperature and high-pressure (HTHP)[76–77], high-energy particle radiation[78], carbide etching[79], and novel synthesis methods (e.g., microplasma dissociation of ethanol vapour[80]) have also been employed. The morphology, size, and properties are significantly influenced by the synthesis method (Table 1). The synthesis can be achieved through diverse methodologies, and the selection of an appropriate synthesis method is contingent on factors such as specific application requirements and production costs[81]. Future research should prioritize the enhancement of controllability and the reduction of synthesis costs to foster the adoption of NDs in diverse fields.

3 Strategies for enhancing ND photocatalysis

NDs as robust photocatalytic platforms, hold exceptional atomic scale durability and tailorable surface functionalities. The sp^3-hybridized crystalline matrix enables diamond to generate high-energy charge carriers under UV excitation, effectively facilitating the photoreduction of molecular nitrogen[83–84] and carbon dioxide[85–86]. Nevertheless, the intrinsic wide bandgap and ultrafast electron–hole recombination kinetics severely hamper their practical implementation in solar-driven catalysis. To circumvent these limitations, precisely engineered modifications have been strategically developed: surface functionalization, plasmonic hybridization, heteroatoms doping, and heterostructure construction. These synergistic approaches collectively address the spectrum-response mismatch and charge dynamics bottleneck that constrain pristine NDs.

3.1 Surface functionalization

The photocatalytic functionality of diamond is primarily dictated by its surface termination, which provides tunability of its electron affinity (χ) across an extremely wide range. This tunability is achieved through surface functionalization using various elements (hydrogen (H), oxygen (O), fluorine (F), chlorine (Cl), magnesium (Mg)) or organic molecules (hydroxyl (OH), phenyl, long-chain amines)[87-93]. These terminations create distinct electronic configurations through interfacial dipole engineering. Crucially, the type of termination dramatically alters the electron affinity: fluorine/oxygen-terminated diamond exhibits positive electron affinity (PEA), while hydrogen-terminated and magnesium-terminated surfaces demonstrate negative electron affinity (NEA) characteristics. Terminations with high electronegativity (like O or F) increase the PEA, pulling electrons towards the surface. Conversely, terminations with lower electronegativity (like H or Mg) result in the NEA, facilitating electron emission into the vacuum[94]. This remarkable electronic adaptability establishes diamond as a uniquely versatile platform for photocatalysis design, enabling tailored electronic properties for specific reactions.

The surface termination of diamond dictates its interfacial dipole: hydrogen termination (ND—H) forms $C^{\delta-}—H^{\delta+}$ dipole, while oxygen termination reverses this to $C^{\delta+}–O^{\delta-}$ (Fig. 6a). ND—H is particularly advantageous for photocatalysis due to its favorable dipole orientation, which facilitates electron emission at solid-liquid interfaces[37]. Its electronic structure features a valence band maximum (VBM) at 5.0 eV and a conduction band minimum (CBM) at +0.5 eV relative to vacuum level[95]. Crucially, the CBM lies above the vacuum level (Fig. 6b). During

Table 1 Comparison of the properties of different preparation methods for ND

Method	Structural Characteristic	Advantage	Limitation	Ref.
Detonation	Core-shell structure 2–10 nm, surface groups	Low cost, scalable	Impurity-prone	[49–50, 52–53]
CVD	Films/discrete particles, less defects	Controlled purity/crystallinity	Slow growth, limited substrate	[57-60]
Laser ablation	sp^3>90%, 3–8 nm, well-dispersed	Rapid, no-purity	Low yield	[63-66]
Cavitation	sp^3 core, amorphous carbon coating	Mild conditions	Poor crystallinity	[67-70]
Ball milling	Irregular shape, mixed sp^2/sp^3 phases	Simple process, adjustable size	Defects, size polydispersity	[73-75, 82]
HTHP	sp^3>99%, >50 nm, H-teminations	High crystallinity, suitable for doping	Costly, wide size distribution	[76–77]

bandgap excitation, this unique configuration enables barrier-free ejection of conduction-band electrons into aqueous media, generating potent reducing agents: hydrated electrons (e^-_{aq}) [96–97]. These metastable species exhibit microsecond-scale lifetimes in water and represent the strongest known reducing agents in aqueous systems. Despite their transient nature in reactive environments, they drive diverse photocatalytic reductions[98–100].

To figure out the potential of ND—H as an advanced photocatalyst, comparative analysis of electron emission behavior among ND—H, carboxylated (ND—COOH), and hydroxylated (ND—OH) surfaces reveals termination-dependent photoresponse

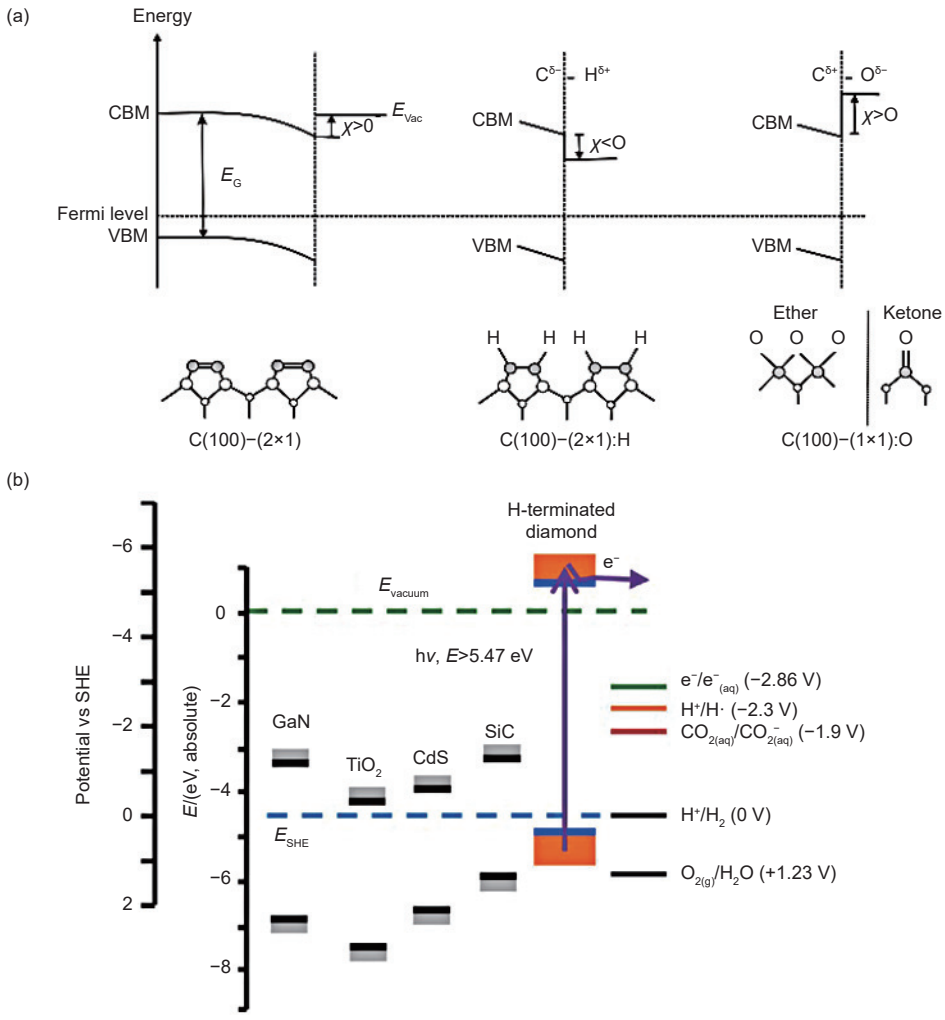

Fig. 6 (a) Band scheme and electron affinity χ for the bare, the hydrogenated, and the oxidized diamond (100) surface[94]. Copyright © 2014 Elsevier. (b) Energy band diagram of H-terminated diamond and some other semiconductors[85]. Copyright © 2017 Elsevier

characteristics (Fig. 7a). Experimental investigations employing deep ultraviolet (DUV: 225 nm, 5.5 eV) and visible light (VIS: 400 nm, 3.1 eV) excitation demonstrate that while all surface terminations exhibit e^-_{aq} emission under DUV irradiation, only ND—H maintains this capability under VIS illumination. The universal DUV response originates from the relative energy alignment between the water CBM and diamond surfaces, where the aqueous phase CBM resides below those of ND—OH, ND—COOH and ND—H[101]. This configuration enables electron transfer across the interface regardless of termination. The superior VIS responsiveness of ND—H stems from two synergistic factors: NEA advantage and hybrid sp^2/sp^3 architecture. Raman spectroscopy reveals the presence of conjugated sp^2 carbon phases within ND—H, creating intra-bandgap states that enable visible light absorption[95,101].

ND—H has been applied to particularly drive reduction reactions such as N_2 conversion, hydrogen evolution, environmental remediation under ambient conditions. Although the intrinsic mechanism requires further elucidation, experimental evidence confirms the critical role of e^-_{aq} generated through sub-band gap irradiation of ND—H in mediating these reduction reactions[102]. Zhu et al.[84] demonstrated that photoexcited ND—H acted as a solid-state electron source, emitting electrons directly into aqueous solu-

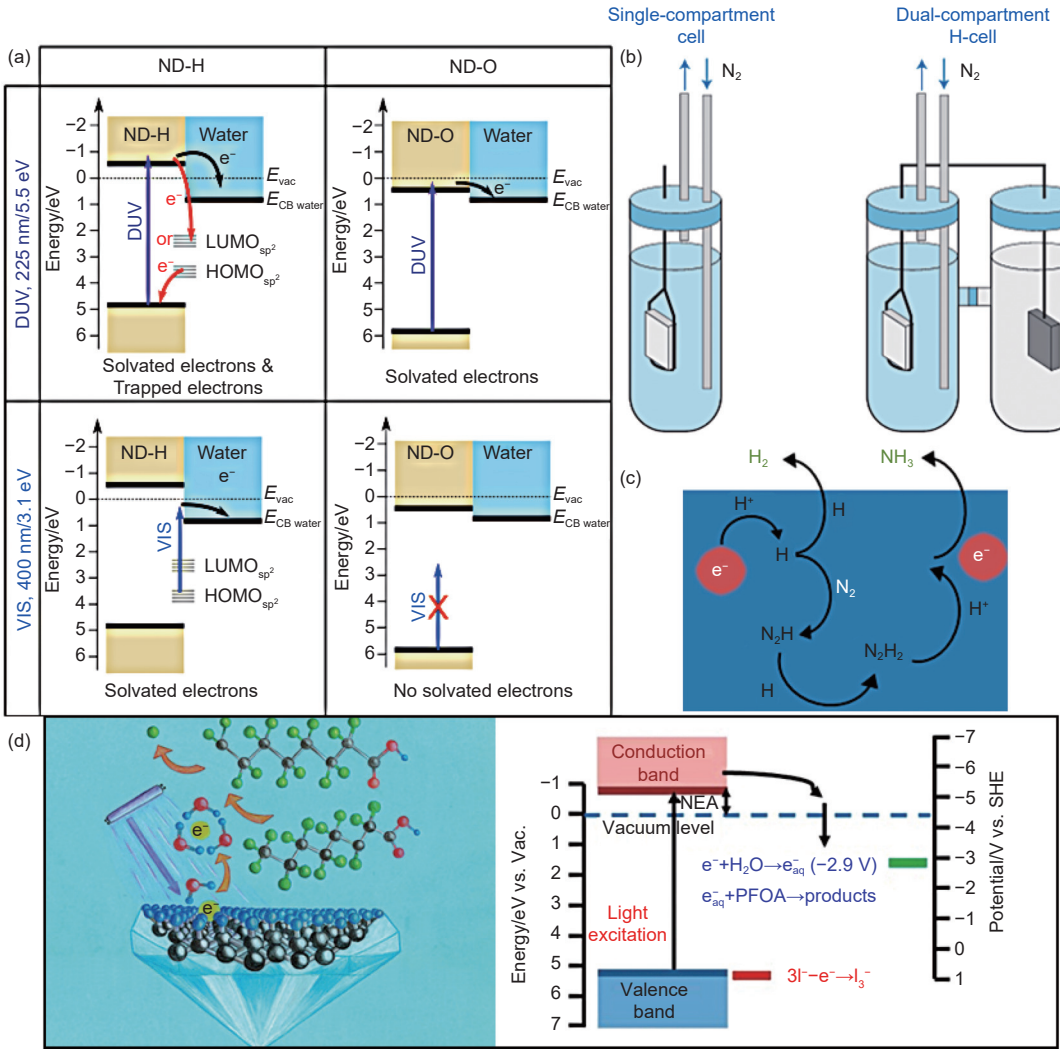

Fig. 7 Schema of (a) e^-_{aq} emission process on ND–H and ND–O under DUV/VIS[101]. (b) Schematic diagram of N_2 photocatalytic reaction vessels[84]. Copyright © 2013 Springer Nature. (c) Proposed mechanism for N_2 reduction by e^-_{aq} [83]. Copyright © 2014, American Chemical Society. (d) Diamond system for PFOA degradation mediated by e^-_{aq} [98]. Copyright © 2022, American Chemical Society

tion. This enabled ambient-temperature photocatalytic ammonia synthesis by N_2 reduction in a single/dual-compartment cell (Fig. 7b). Transient absorption spectroscopy confirmed the presence of e^-_{aq} near the diamond surface after photoexcitation. Combined experimental and computational analyses (including electronic structure calculations, molecular dynamics, kinetic modeling) revealed a dual-path reduction mechanism (Fig. 7c): initial steps proceeded by direct hydrogen atom addition (HAA), while later stages involved sequential protonation and direct reduction by e^-_{aq} [83]. This HAA-initiated, protonation/electron-transfer mechanism is the only plausible route for N_2 reduction by aqueous solvated electrons generated from diamond. Jang et al.[103] demonstrated that hydrogen-treated NDs exhibited enhanced quantum yields in photocatalytic hydrogen evolution under 532 nm pulsed laser irradiation, attributing this improvement to hydrogen atoms functioning as effective electron reservoirs during multiphoton absorption processes. Liu et al.[98] achieved efficient degradation of persistent pollutants such as perfluorooctanoic acid (PFOA) under high-energy UV excitation, proposing a mechanism involving bandgap-induced hydrated electron generation (Fig. 7d).

As an alternative to ND—H, surface modification with primary amino groups has emerged as an effective strategy to create oxidation-resistant, positively charged diamond surfaces. Zhu et al.[104] pioneered a robust methodology for fabricating amino-terminated diamond (ND—NH_2) surfaces with preserved NEA, demonstrating their capacity to emit electrons into aqueous solutions for nitrogen reduction. Comparative analysis of NH_3 production, in Fig. 8a, reveals that ND—NH_2 exhibits moderately enhanced catalytic performance over ND—H, with acid-treated ND—NH_2 surfaces (HCl immersion) showing substantially improved yields. This trend aligns with vacuum-phase electron emission behavior, confirming the universality of the emission mechanism. The enhanced functionality arises from protonation of surface-bound —NH_2 groups to —NH_3^+ under

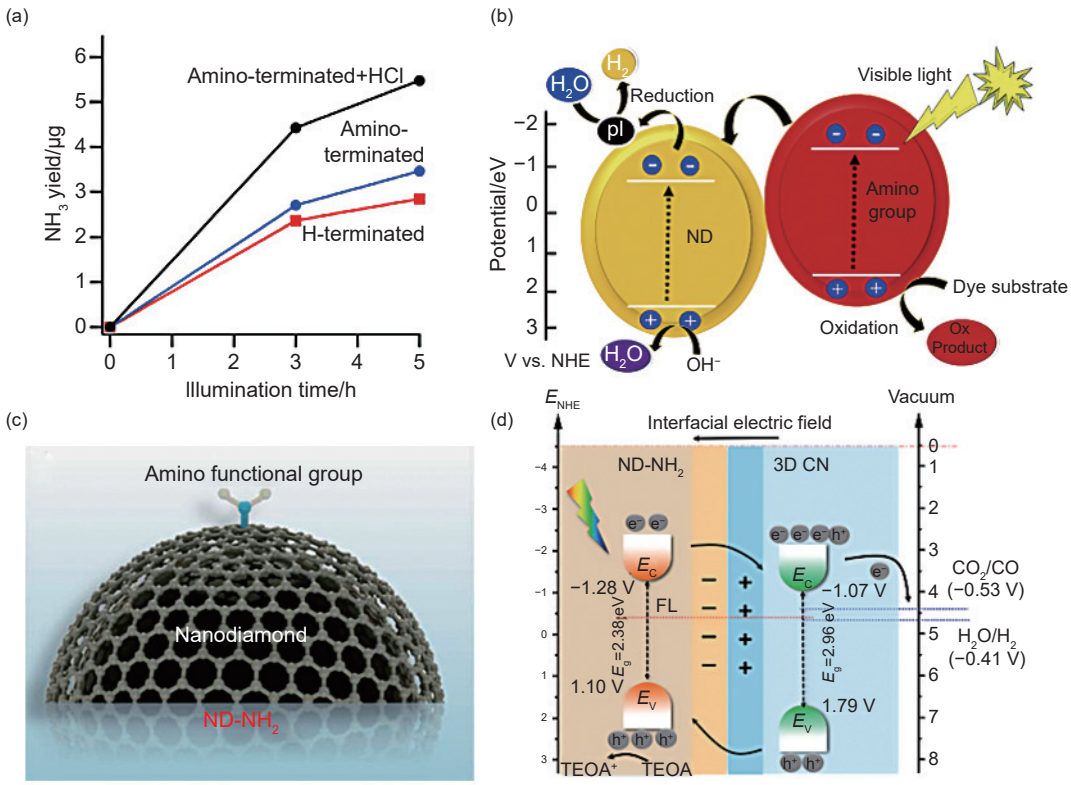

Fig. 8 (a) Ammonia yield results for ND–H, ND–NH_2 and acid-treated ND–NH_2[104]. Copyright © 2016, Elsevier. (b) Photocatalytic mechanism proposed for ND–NH_2 under solar light[105]. Copyright © 2020, Elsevier. (c) Schematic illustration of ND–NH_2. (d) Proposed mechanism of photocatalytic reduction of CO_2 by 3D CN@ND–NH_2[16]. Copyright © 2024, Royal Society of Chemistry

ambient pH conditions, which facilitates electron transfer kinetics. The integration of amino groups into ND matrices induces 3 synergistic effects: (1) Enhanced visible light absorption through modified electronic transitions. (2) Increased specific surface area providing abundant reaction sites. (3) Improved charge separation by amino/ND heterojunction formation. As illustrated in Fig. 8b, this functionalization promotes efficient transition of photogenerated carriers from ground to excited states, significantly boosting photocatalytic hydrogen evolution and pollutant degradation under visible light irradiation[105].

Recent advancements in heterostructure engineering further demonstrated the versatility of amino-functionalized ND. Our group developed a three-dimensional g-C_3N_4@ND—NH_2 composite exhibiting exceptional CO_2 photoreduction performance (Fig. 8c, d)[16]. The ND—NH_2 component enhanced light harvesting efficiency while optimizing carrier separation through type-II heterojunction formation. Type-II heterojunctions facilitated spatial charge separation through staggered band alignment: Electrons transfered from the conduction band of ND—NH_2 to the valence band of 3D CN, while holes migrated in the opposite direction, enabling separated redox sites. Comparative studies confirmed superior gas adsorption capacity and long-term stability in the 3D CN@ND—NH_2 system, establishing amino-functionalization as a critical design parameter for advanced photocatalytic architectures. Hence, surface-engineered NDs, through hydrogen termination or amino functionalization, establish tailorable electron-emitting functionality that drives versatile reduction catalysis, with protonation-modulated charge transfer being pivotal for reaction kinetics optimization.

3.2 Plasmonic hybridization

To address the inherent energy gap limitation of ND, innovative integration with plasmonic nanostructures (e.g., Au, Ag, Cu, Al) has emerged as a groundbreaking strategy through localized surface plasmon resonance (LSPR) engineering[106-108]. This approach capitalizes on plasmonic sensitization to extend the optical responsiveness of diamond-based semiconductors into the visible spectrum, a methodology extensively validated for enhancing light harvesting in conventional photocatalytic materials[109]. When plasmonic nanostructures are incorporated into photocatalytic systems or photoelectrodes, they modulate reaction efficiency by multiple synergistic mechanisms: (1) enhanced broadband light absorption; (2) far-field light scattering to extend photon propagation paths; (3) near-field electromagnetic field at material interfaces; (4) generation of energetic hot carriers through non-radiative plasmon decay; and (5) plasmonic heating effects that alter local reaction kinetics. These plasmon-driven phenomena profoundly influence critical semiconductor processes, including photon harvesting, charge carrier separation, migration, recombination dynamics, and interfacial charge transfer to redox species in electrolytes[110–111]. The employment of suitable co-catalysts, typically noble metals, can further enhance charge extraction while suppressing recombination losses at active sites.

NDs, with high surface area-to-volume ratio (e.g., 300–400 $m^2\ g^{-1}$ for 4–6 nm NDs) and abundant surface defect sites (e.g., sp^2/sp^3 hybridization boundaries), provide optimal platforms for anchoring metal atoms. Furthermore, the distinctive electronic structure enables precise modulation of catalytic activity and selectivity by metal-support interactions[112–113]. Yadav et al.[114] engineered strontium titanate (STO) photocatalysts modified with NDs and Ru cocatalysts for efficient CO_2-to-CO conversion. Fig. 9a proposed the mechanism: (1) Light excitation generated electron-hole pairs in both STO (CBM = 0.14 eV) and NDs (CBM = 0.37 eV). (2) Electrons from STO's lower CBM recombined with holes in NDs' higher VBM (2.51 eV vs. STO's 3.14 eV), suppressing recombination. (3) Photoexcited electrons accumulated in NDs' CBM and migrated to STO's lower CBM and adjacent Ru sites. (4) Electron-enriched Ru ions efficiently reduced CO_2, while charge separation preserved reactive holes in STO/NDs for sustained catalysis. Orlanducci et al.[115] demonstrated that visible light-induced e^-_{aq} generation efficiency was enhanced by growing gold nanoparticles on dispersed DNDs (AuNPs@DNDs) in water (Fig. 9b). Production was

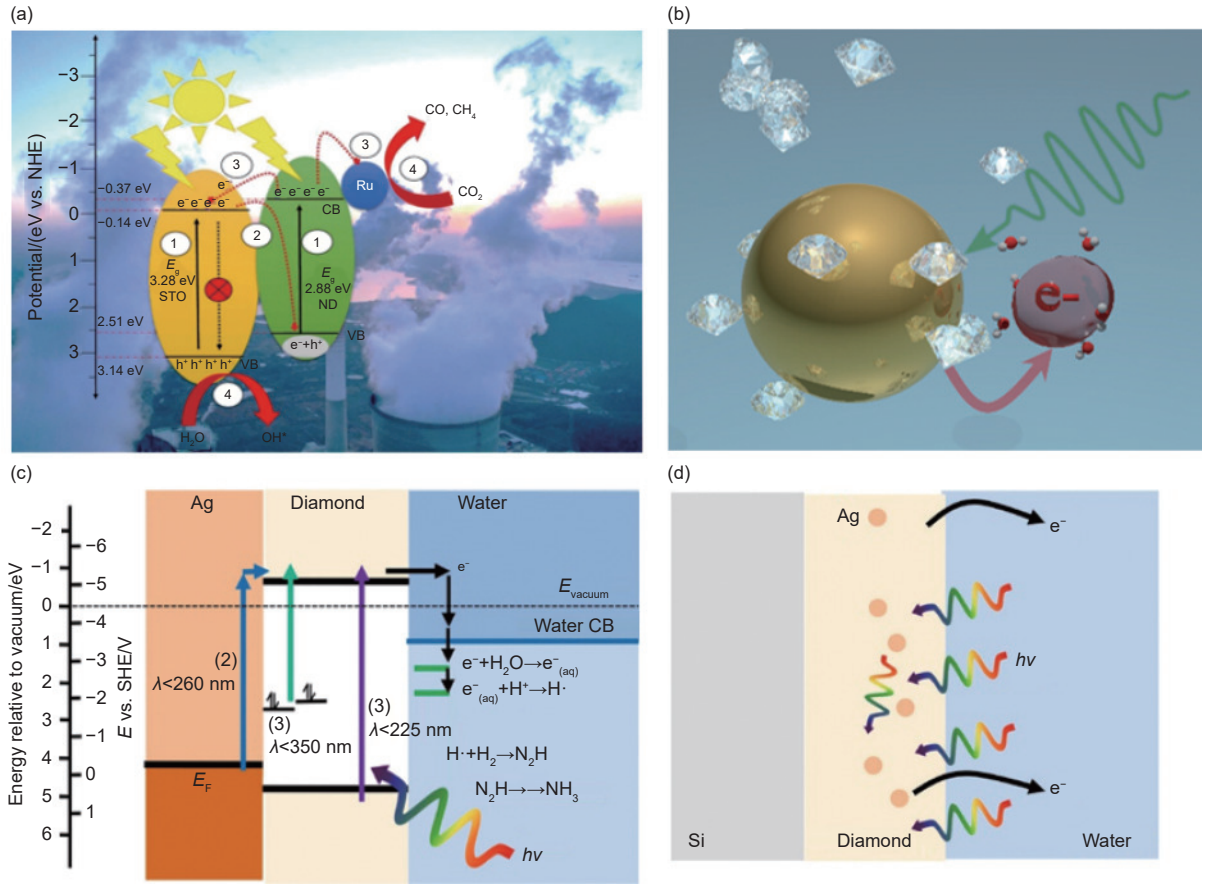

Fig. 9 (a) Proposed mechanism for the photocatalytic CO_2 hydrogenation upon STO—ND—Ru composite[114]. Copyright © 2023, Elsevier. (b) Scheme of AuNP@DNDs emitting electrons[115]. Copyright © 2024, American Chemical Society. (c) Three pathways of enhancing diamond photocatalysis with Ag nanoparticles in the reduction of N_2. (d) Scheme of Ag nanoparticles as scattering centers to enhance electron emission[116]. Copyright © 2018, American Chemical Society

monitored by transient absorption spectroscopy at 700–750 nm. Optimizing this process held significant potential for advancing energy-intensive solar photocatalysis, such as N_2 and CO_2 reduction, and providing non-toxic e^-_{aq} sources for wastewater treatment and nanomedicine.

The integration of silver nanoparticles with NDs demonstrates exceptional broadband light absorption extending into the near-infrared spectrum. As evidenced by Li et al.[116], embedding Ag nanoparticles within diamond films significantly enhanced photocatalytic activity by synergistically improving light harvesting and mediating solvated electron-driven reduction of N_2 to NH_3 in aqueous environments. Three pathways enhanced diamond photocatalysis with Ag nanoparticles (Fig. 9c): (1) Direct bandgap excitation (λ < 225 nm): enhanced by Ag-induced light scattering, increasing deep-UV optical path length. (2) Internal photoemission (λ < 260 nm): sub-bandgap photons excited electrons from Ag's valence band to diamond's conduction band (~ 0.5 eV above vacuum). (3) Defect-mediated excitation (340–360 nm): sub-bandgap photons promoted electrons from localized sp^2-hybridized graphitic impurities to the conduction band. This wavelength range coincided with Ag plasmonic resonances, suggesting potential synergy. Remarkably, sub-bandgap excitation (λ > 225 nm) coupled with Ag nanoparticle doping induced a fivefold activity enhancement, underscoring the critical role of internal photoemission in expanding the operational wavelength beyond the intrinsic diamond bandgap (Fig. 9d). Additionally, this innovative architecture employed functionalizable ND surfaces as inert substrates for anchoring plasmonic Ag nanoparticles, creating a directly photoactive hybrid system. The optimized composite exhibited exception-

al visible-light-driven degradation of methylene blue (MB) with a rate constant of 28.4 s^{-1} g^{-1}, a benchmark advancement in plasmon-enhanced photocatalysis[117]. Mechanistic analyses revealed that LSPR-mediated energy transfered from Ag nanoparticles drives MB decomposition, while the ND support amplified degradation kinetics through synergistic charge modulation. Further extending this paradigm, hydroxyl-functionalized ND-supported Ag nanoparticles demonstrated versatile sunlight-driven photocatalytic activity for decolorizing synthetic dyes[118]. Generally, plasmonic-ND hybrids establish multifunctional platforms where synergistic LSPR effects, interfacial charge modulation, and defect engineering collectively overcome spectral constraints to achieve record solar fuel and remediation efficiencies.

3.3 Heteroatom doping

Heteroatom doping serves as a critical strategy for bandgap engineering in NDs, enabling tailored electronic structure modification through the introduction of mid-gap impurity states. These dopant-induced energy levels extend optical absorption into visible wavelengths while strategically modulating charge carrier dynamics. The effectiveness of this approach in enhancing visible-light responsiveness has been extensively validated across conventional semiconductor photocatalysts, including benchmark materials such as TiO_2[119–120] and ZnO[121]. The fundamental mechanism involves bandgap narrowing through the formation of intermediate energy states between the valence and conduction bands. Dopant species function as charge-trapping centers, isolating photogenerated carriers from band recombination pathways and promoting their diffusion to active surface sites. However, excessive dopant concentrations must be avoided, as they introduce crystallographic defects

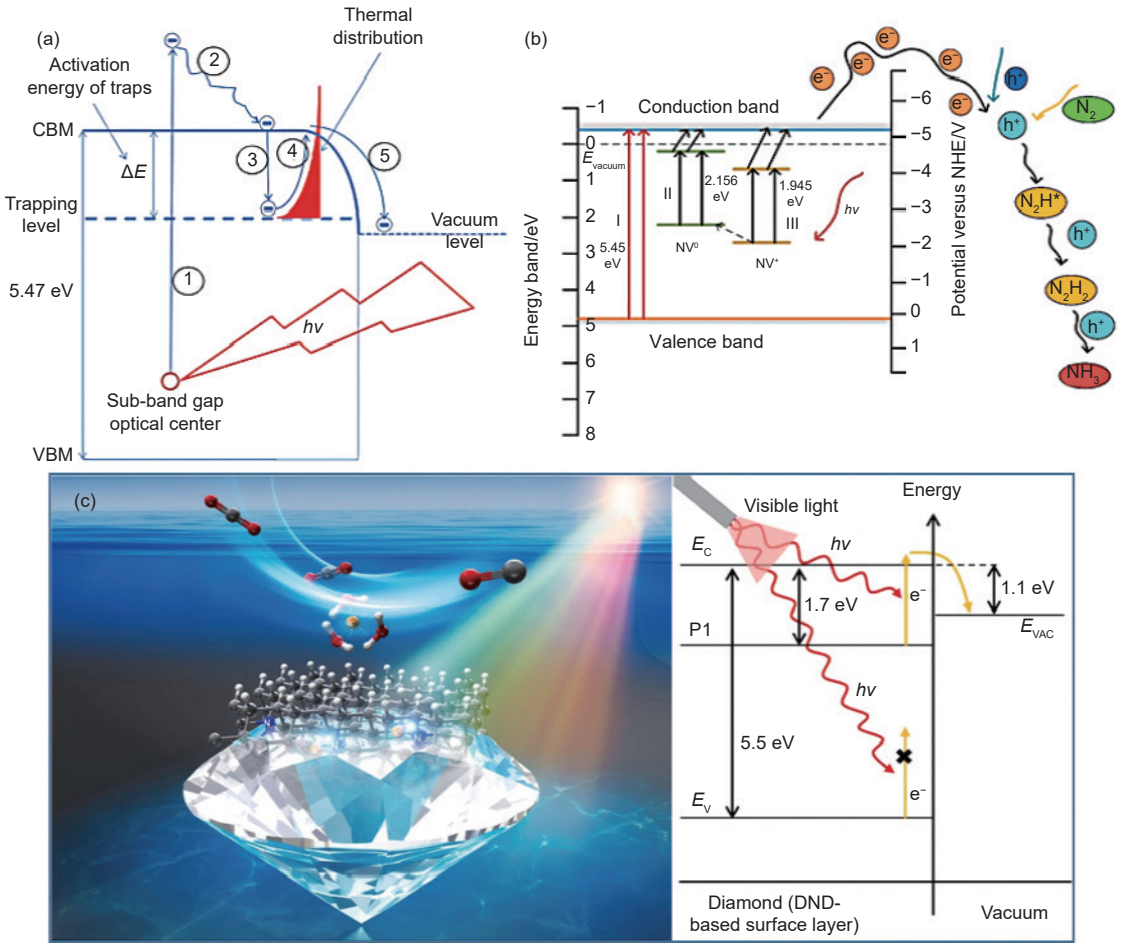

Fig. 10 (a) ta-PETE model[122]. Copyright © 2017, Elsevier. (b) The schema of the influence of nitrogen levels on diamond photocatalysis[123]. (c) Energy diagram of the electron-excitation surface layer[124]. Copyright © 2024, Elsevier

that act as charge recombination centers—counterproductively diminishing photocatalytic efficiency.

Boron and nitrogen emerge as predominant dopants for NDs due to their atomic radii compatibility with carbon. Elfimchev et al.[122] systematically investigated visible sub-band gap photoelectron emission (PEE) of polycrystalline diamond films in the wavelengths range of 360–520 nm. Nitrogen correlation centers were the main source of PEE, while nanocrystalline diamond had a low emission efficiency due to the presence of a large number of defects. The trap-assisted photoenhanced thermoelectron emission (taPETE) model was demonstrated in Fig. 10a, to elucidate the enhanced emission efficiency of nanocrystalline diamond at elevated temperatures and to estimate the activation energies of the trap energy levels of different diamond films. The photoelectrons were trapped by shallow traps, followed by thermal excitation at elevated temperatures and escape into the vacuum. Su et al.[123] demonstrated nitrogen-doped NDs as efficient photocatalysts for visible-light-driven ammonia synthesis. Controlled nitrogen doping engineered nitrogen vacancy (NV) centers, extending diamond's photoresponse beyond intrinsic bandgap absorption observed near 220 nm. This doping broadened the optical absorption spectrum, significantly enhancing overall absorbance and generating new impurity-induced characteristic absorption bands at ~ 320 nm and ~ 460 nm. Mechanistic studies revealed that NV centers facilitated internal photoemission, exciting electrons to conduction band edges and generating substantial UV and visible-range photocurrents (Fig. 10b). Critical insights into defect-mediated interband transitions and surface reaction pathways were established, particularly relevant for weakly adsorbing molecules like N_2 and CO_2. Recent breakthroughs by Yoshikawa et al.[124] further exemplified nitrogen doping's potential, showcasing heavily doped diamond nanolayers (N density $\geqslant 10^{21}$ cm^{-3}) for visible-light-driven CO_2 reduction. In diamond containing nitrogen-associated defects (Fig. 10c), visible light (activation energy below ~ 3.5 eV) promoted electrons from these mid-gap electronic states into the conduction band. These photoexcited electrons subsequently ejected into vacuum by NEA surfaces. Thus, strategic nitrogen doping creates defect-mediated bandgap engineering, enhanced carrier dynamics, and tailored surface reactivity, which is critical for activating inert molecules in solar fuel production.

3.4 Heterostructure construction

The limited solar spectrum utilization and rapid charge recombination inherent in conventional semiconductors have motivated the development of ND-based hybrid photocatalysts. By strategically integrating NDs with metal oxides (e.g., TiO_2[125], ZnO[126]), nitrides (e.g., C_3N_4[127]), and transition metal oxides (e.g., WO_3[128], Cu_2O[129]), type-II heterojunctions have been constructed to exploit interfacial built-in electric fields toward efficient spatial charge separation. This synergistic design effectively addresses critical limitations: (1) mitigating photocorrosion and enhancing the photocatalytic stability[126]; (2) facilitating rapid capture of photogenerated carriers in the adjacent semiconductor, thereby promoting charge separation[130]; and (3) strengthening visible-light absorption and providing additional reactive sites[128]. For instance, Lin et al.[129] enhanced the photocatalytic hydrogen production performance of ND by embedding it within p-type cuprous oxide (Cu_2O) nanocrystals (Fig. 11a). The ND@Cu_2O composites achieved hydrogen production rates of 1597 and 824 μmol g^{-1} h^{-1} under simulated solar and visible light irradiation, respectively, and their solar-to-hydrogen conversion efficiency was 0.85%, which was nearly 10 times higher than that of pure Cu_2O. The enhanced performance was attributed to the electron supplying ability of ND and the alignment of the energy band structure with that of Cu_2O, facilitating electron injection from ND into Cu_2O. In the ND/Cu_2O heterojunction, staggered band alignment created favorable thermodynamics for charge transfer: Valence Band (VB): ND (1.45 eV) < Cu_2O (1.77 eV vs. NHE), Conduction Band (CB): ND (−0.76 eV) > Cu_2O (−0.63 eV vs. NHE). This configuration could drive electron transfer from ND to Cu_2O under irradiation. However, ND's electron-donating capability, enabled by oxygen functional groups, was

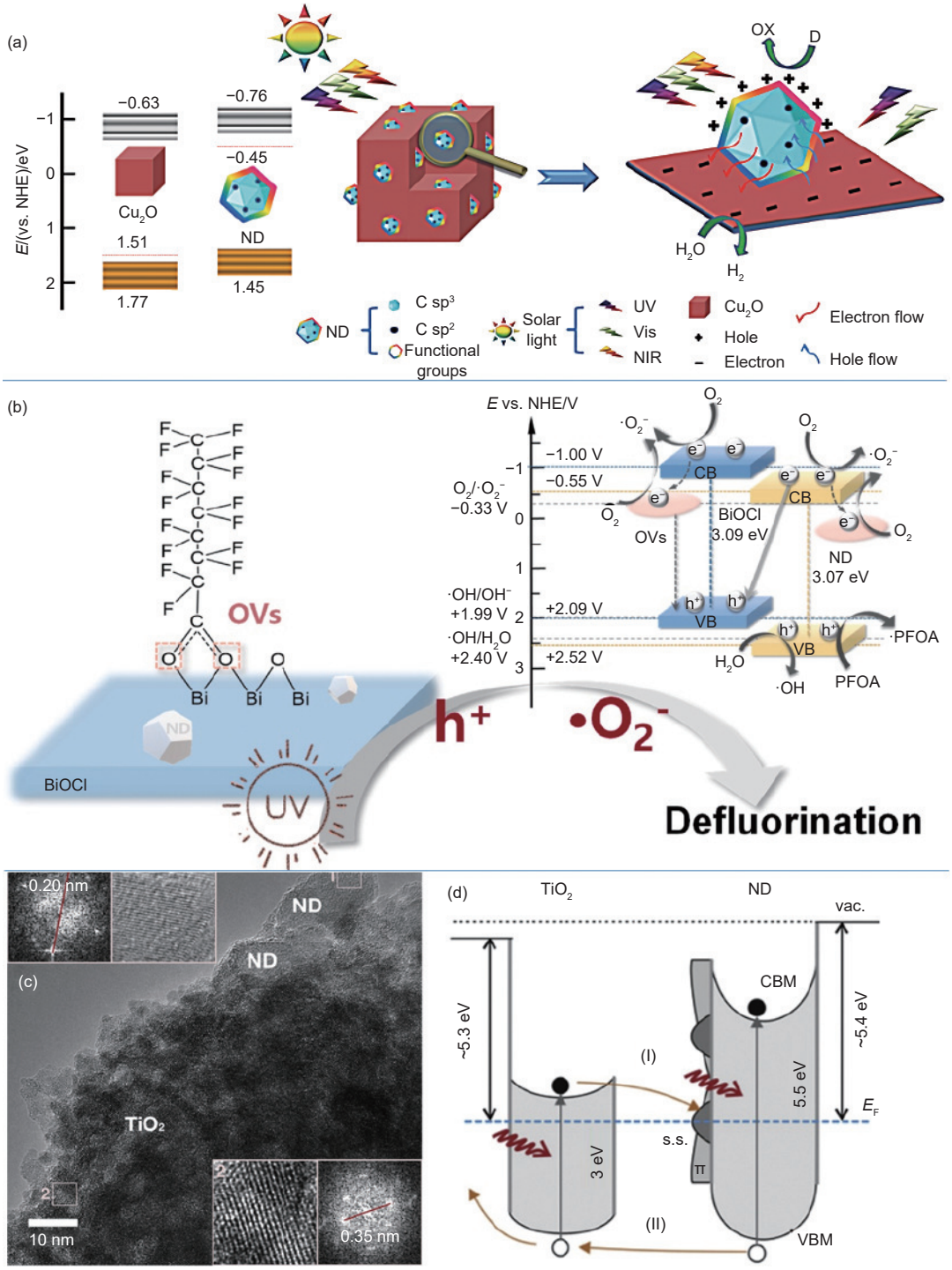

Fig. 11 Photocatalytic mechanism of (a) H_2 evolution by NDs@Cu_2O[129] ("D" and "OX" mean electron donor and oxidation products), and (b)PFOA degradation by BiOCl@ND[131]. Copyright © 2015, John Wiley and Sons. Copyright © 2024, Elsevier. (c) TEM image of pure TiO_2, ND and TiO_2@ND. (d) Scheme of band energy levels and charge transfer process in the TiO_2@ND under illumination[132]. Copyright © 2019, Elsevier

critical for realizing this charge separation. Without these surface-mediated donor states, photogenerated carriers recombined internally despite thermodynamically favorable band offsets. Thus, surface functionalization governs both spectral response and interfacial charge kinetics in the hybrid system.

In general, ND-based composite potocatalysts have been applied primarily in two domains: (1) environmental remediation (e.g., pollutant degradation) and (2) solar fuel conversion (e.g., hydrogen evolution, CO_2 reduction). NDs show significant promise in environmental remediation, functioning both as ad-

sorbents and photocatalysts to effectively remove a wide range of contaminants, including heavy metals, organic pollutants, and dyes. ND-based composites consistently exhibit superior photocatalytic performance compared to pristine NDs. Xu et al.[131] synthesized BiOCl@ND composites (Fig. 11b), achieving complete PFOA degradation within 60 min under UV irradiation, with a rate constant 3.8 times higher than that of pure BiOCl. The proposed mechanism for PFOA decomposition at the BiOCl-ND heterojunction involves several key steps: (1) strong interfacial coordination between PFOA molecules and the catalyst surface promotes direct interaction; (2) UV excitation generates electron-hole pairs in both BiOCl and ND; (3) the heterojunction facilitates directional charge separation, with electrons migrating to the ND conduction band and holes remaining in the BiOCl valence band; (4) oxygen vacancies (OVs) in both components trap photogenerated electrons, suppressing recombination; and (5) direct hole oxidation in BiOCl's valence band decomposes PFOA into unstable perfluorinated carboxylic radicals, triggering degradation. This synergistic mechanism, combining interfacial engineering, charge separation, and defect-assisted trapping, drives radical-mediated PFOA decomposition with high efficiency. Similarly, Henych et al.[132] developed TiO_2@ND composites (Fig. 11c) for enhanced photocatalytic toxin degradation. The NDs improved activity through 2 synergistic mechanisms (Fig. 11d). Route I, spatial charge separation, wherein photogenerated electron-hole pairs in TiO_2 separate at the TiO_2/ND interface. NDs act as electron acceptors owing to favorable band alignment (the TiO_2 vacuum level is ~ 0.1 eV lower), forming an electron-depletion region in TiO_2 and reducing recombination losses. Route II, defect-mediated photosensitization, in which NDs absorb light by defects or surface states, generating additional holes that transfer to TiO_2 by favorable band bending. Upon contact, Fermi level equilibration occures, enhancing charge transport. Both mechanisms contribute to increased photovoltage, suppressed recombination, and enhanced hole availability, as confirmed by DRIFTS and surface potential analysis. Collectively, these findings highlight the pivotal role of NDs in optimizing charge separation and interfacial electron dynamics to enhance photocatalysis performance. Nonetheless, discrepancies arising from light-source dependency and challenges in process scalability remain critical obstacles that must be overcome to translate laboratory success into practical applications.

In the solar conversion for hydrogen energy production, heterojunction photocatalysts based on g-C_3N_4 and NDs have demonstrated considerable promise in photocatalysis. The graphitic carbon nitride is a metal-free semiconductor that presents physicochemical stability and cost-effectiveness, negligible toxicity, and suitable CB energy as well as easy preparation from various precursors[133]. However, its practical applications are constrained by inherent limitations including partial visible-light absorption (attributed to its moderate bandgap), rapid electron-hole recombination, and insufficient active sites[134]. Recent advancements demonstrate that constructing heterojunctions with NDs (g-C_3N_4@ND in Fig. 12a) effectively addresses these challenges while maintaining the metal-free photocatalytic system[135–136].

For instance, a mesoporous DND-modified g-C_3N_4 system exhibited 50% higher hydrogen evolution than pristine g-C_3N_4, attributed to improved charge transfer, increased surface area, and suppressed carrier recombination[137]. Su et al.[38] pioneered a one-step pyrolysis synthesis of g-C_3N_4@ND heterostructures, achieving a 5.6-fold enhancement in visible-light photocatalytic water splitting efficiency through optimized light scattering and interfacial charge separation. As shown in Fig. 12b, UV-vis diffuse reflectance spectra revealed that while pristine g-C_3N_4 exhibited an absorption edge at ~ 455 nm (band gap = 2.72 eV), the g-C_3N_4@ND heterostructures displayed significantly broadened absorption across the measured wavelength range. This enhancement was primarily attributed to intensified light scattering at the g-C_3N_4/ND interfaces. Subsequent developments incorporated boron-doped NDs[138] and hierarchical structures with silver nanoparticles[139], demonstrating

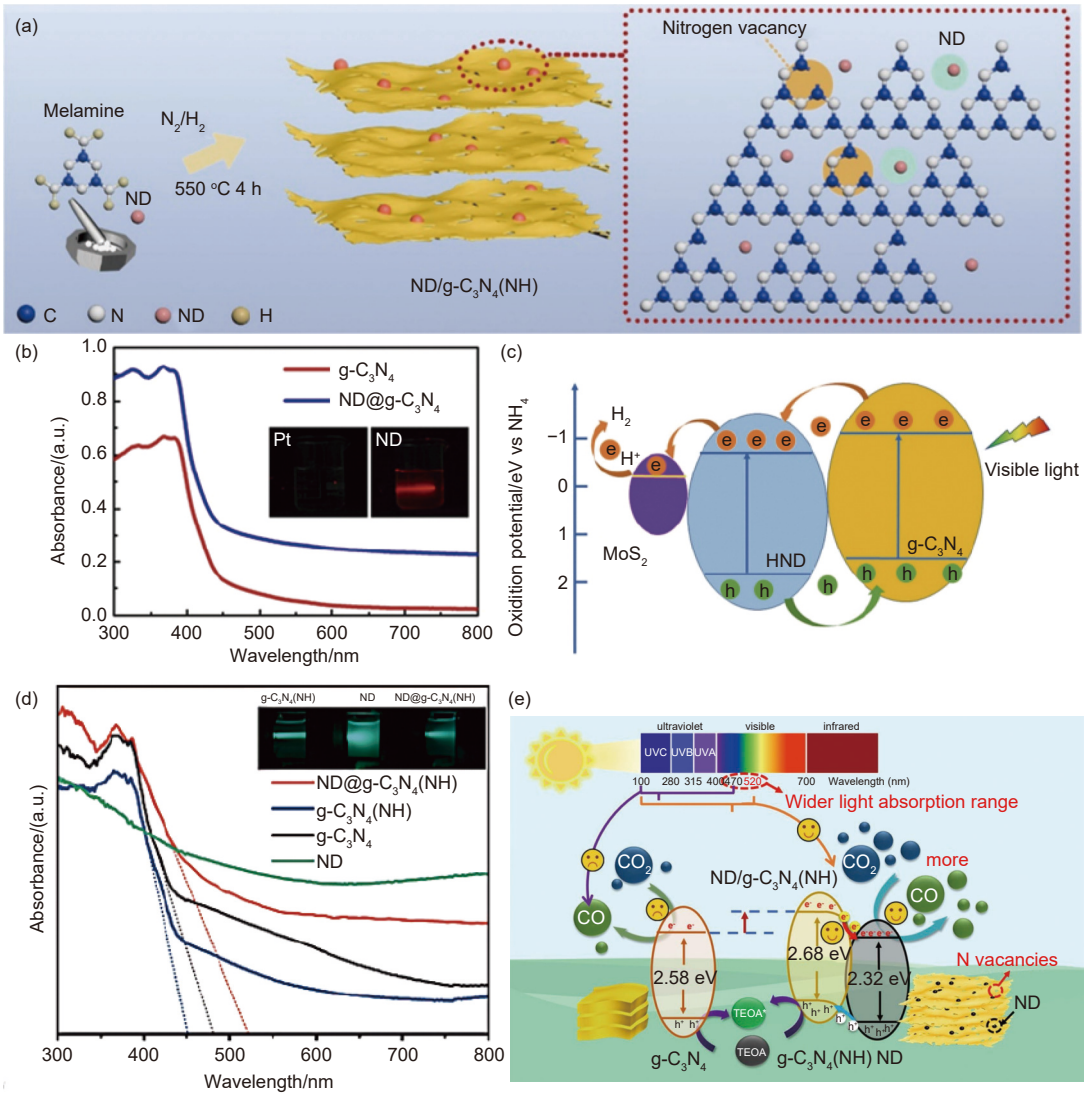

Fig. 12 (a) Preparation process for ND/g-C_3N_4(NH).[141] (b) UV-vis spectra of the g-C_3N_4 and ND@g-C_3N_4 heterostructures[38]. Copyright © 2018, Elsevier. (c) Photocatalytic mechanism for hydrogen evolution over MoS_2/HND/g-C_3N_4.[140] Copyright © 2024, Elsevier. (d) UV-vis spectra and corresponding scattering effect (insert)[141]. (e) Photocatalytic mechanism of ND/g-C_3N_4(NH) for CO_2 reduction[141]. Copyright © 2022, Elsevier

4.9-fold and 2.4-fold improvements in hydrogen evolution and pollutant degradation, respectively, by synergistic plasmonic and optical confinement effects. The most recent innovation by Su et al.[140] introduced MoS_2 quantum dots into a hybrid g-C_3N_4@ND system (Fig. 12c), achieving remarkable hydrogen production rates (227 μmol g^{-1} h^{-1}) through combined light scattering and co-catalytic mechanisms under visible light irradiation ($\lambda \geqslant 420$ nm).

In addition to hydrogen production, heterostructured g-C_3N_4@ND has demonstrated remarkable efficacy in CO_2 photoreduction. Gao et al.[16] embedded ND—NH_2 into 3D porous g-C_3N_4 (3D-CN) by a two-step self-assembly method to form a 3D-CN@ND—NH_2 heterojunction for photocatalytic CO_2 reduction. The photocatalytic CO generation was increased by 1.97-fold and the cycling test showed excellent chemical stability. Among them, ND—NH_2 increased the alkalinity of 3D-CN and promoted CO_2 adsorption, the narrow bandgap (2.86 eV) of the type II heterojunction enhanced light absorption, and the built-in electric field accelerated electron-hole separation. This work solved the efficiency and stability challenges of traditional catalysts through the synergistic design of functionalized NDs and 3D-CN, and provided a new idea for metal-free photocatalytic systems. Moreover, Li et al.[141] achieved an 18.6-fold enhancement in CO_2 photoreduction efficiency for g-

C_3N_4 by introducing NVs and ND modification. The introduction of NVs optimized the material's conduction band position, and ND decoration expanded the light absorption range, compensating for the insufficient absorption inherent to the layered structure. The decoration of ND critically improved performance by: (1) extending light absorption end to 520 nm by scattering effects (Fig. 12d); (2) reducing the composite bandgap through the chemical bonding of the sp^2 hybridized carbon in the ND with the π-conjugated structure of the g-C_3N_4(NH) melon units; (3) enabling efficient charge separation by a Type-II heterojunction; (4) Enhancing CO_2 adsorption and electron utilization at ND sites. Together, these ND-driven effects maximized charge separation and reactant activation (Fig. 12e). While these developments highlight the potential of ND@g-C_3N_4 heterojunctions, critical challenges remain in assessing long-term operational stability, scalability of synthesis methods, and comprehensive understanding of multi-component synergistic effects.

4 Summary and outlook

This review systematically examines four principal strategies for enhancing ND-based photocatalysis: (1) Surface termination engineering enables direct electron injection into aqueous media by functionalized interfaces, thereby facilitating barrier-free reduction reactions. (2) Plasmonic hybridization with noble metals extends visible-light absorption through LSPR and simultaneously accelerates interfacial charge-transfer kinetics. (3) Band structure modulation by heteroatom doping narrows the intrinsic bandgap and optimizes carrier dynamics through controlled defect engineering. (4) Heterojunction construction promotes efficient charge separation through precisely tailored band alignments. Collectively, these synergistic approaches markedly improve quantum efficiency by optimizing interfacial electron transfer, spatial charge separation, and recombination suppression. The exceptional tunability of ND interfaces thus enables the rational design of targeted architectures for solar fuel conversion, with Table 2 benchmarking representative ND-baded systems for CO_2 reduction, nitrogen fixation, and water splitting.

Despite significant advances demonstrating the extraordinary potential of carbon-based photocatalytic materials for solar energy conversion, critical challenges persist. (1) The performance of hybrid systems is highly dependent on the intrinsic properties of the carbon components (e.g., defect density, surface functionalization, and synthesis route). Achieving effective interfacial coupling requires optimal semiconductor dispersion, uniform carbon decoration, and well-

Table 2 Performance of ND-based photocatalysts in solar fuel synthesis

Solar conversion	Material system	Light source	Product selectivity/yield	Yield rate	Ref.
CO_2 reduction	N-doped diamond	>387 nm	>90% (CO)	3 μmol cm^{-2} h^{-1}	[124]
	3D CN@ND–NH_2	> 420 nm	1.97-fold CO (vs. COOH–ND)	13.81 μmol g^{-1} h^{-1}	[16]
	STO–ND–Ru	Sunlight	85.6% (CO)	1131.5 nmol g^{-1} s^{-1}	[114]
	ND/g-C_3N_4(NH)	> 420 nm	91.4% (CO)	10.98 μmol h^{-1}	[141]
	ND–H	UV lamp	>75% (CO)	–	[85]
	B-doped diamond	<225 nm	>90% (CO)	–	[37]
H_2 production	Ag/ND/g-C_3N_4	⩾ 420 nm	4.9 times yield (vs. Ag/g-C_3N_4)	158 μmol h^{-1} g^{-1}	[139]
	ND@Cu_2O	solar light	0.85% solar-to-H_2 efficiency	1597 μmol h^{-1} g^{-1}	[129]
	g-C_3N_4/DND	420–620 nm	1.5 times yield (vs. g-C_3N_4)	–	[137]
	ND–H	532 nm laser	higher yield (vs. ND–O)	0.090 mmol h^{-1}	[103]
N_2 reduction	N-doped diamond	200–800 nm	–	6.27 ± 1.48 nmol cm^{-2} h^{-1}	[123]
	NH_2-terminated diamond	UV	higher yield (vs. H–diamond)	–	[104]
	Diamond–Ag–Diamond	UV-Vis (>225 nm)	3.5 times yield (vs. Diamond–Si)	13.31 nmol cm^{-2} h^{-1}	[116]

defined contact interfaces. Thus, advanced synthesis techniques for both pristine carbon materials and carbon-semiconductor hybrids are essential to precisely control these structural and electronic parameters. (2) Interfacial charge-transfer dynamics remain insufficiently understood. Uncertainties persist regarding whether carbon primarily serves as an electron donor or acceptor, as well as the dominant electron-transfer pathways (e.g., conventional Type-II). High-resolution transient spectroscopy and theoretical modeling are urgently needed to elucidate these electronic interactions. (3) Most current studies rely on sacrificial agents for H_2 evolution, whereas practical clean-energy applications demand photocatalytic overall water splitting. Future research should therefore focus on realizing sacrificial-agent-free systems and extend exploration toward CO_2 reduction into hydrocarbon fuels, another pivotal route for sustainable solar-to-chemical energy conversion.

NDs should be strategically applied in areas where conventional photocatalysts encounter intrinsic limitations, particularly in harsh-environment solar fuel production. Their exceptional corrosion resistance enables efficient seawater splitting, overcoming chloride-induced degradation that plagues metal-based catalysts. Meanwhile, hydrogen-terminated NDs exhibit unique proton-blocking properties, facilitating acidic CO_2 conversion processes where traditional catalysts often dissolve. This targeted application leverages NDs' unmatched chemical stability and electron-emission capabilities at solid-liquid interfaces. By focusing on these high-barrier reaction systems, NDs can pave the way for scalable solar fuel generation under practical conditions, advancing both sustainability and real-world viability. Future development should optimize ND-semiconductor interfaces for charge dynamics in extreme pH/salinity, positioning NDs as cornerstone materials for industrial photocatalysis.

Conflict of interest

The authors declare no competing financial interest.

Acknowledgements

We gratefully acknowledge the financial support from the National Key Research and Development Program of China (2024YFF0508500), National Natural Science Foundation of China (52102162), Guangdong Basic and Applied Basic Research Foundation (2022A1515011794), and Shenzhen Science and Technology Program (JCYJ20241202123733043, GXWD20231130110722002).

References

[1] Chen Z, Yu B, Li Y, et al. Assessing the potential and utilization of solar energy at the building-scale in shanghai[J]. Sustainable Cities and Society, 2022, 82: 103917.

[2] Zhou K, Wang Y, Jiang Z, et al. Ir/Mn Co-mixing and oxide-support interaction modulation through plasma promoted asymmetric oxygen coupling for stable acidic oxygen evolution[J]. Advanced Materials, 2025: 2420159.

[3] Zhao Z, Gao X, Zhang H, et al. Multifunctional diamond-based catalysts: promising candidates for energy conversions in extreme environments—a mini-review[J]. Electron, 2024, 2: e45.

[4] Bagheri S, Muhd Julkapli N. Nano-diamond based photocatalysis for solar hydrogen production[J]. International Journal of Hydrogen Energy, 2020, 45: 31538-31554.

[5] Gao X W, Zhao Z W, He Y, et al. Nanodiamond: a promising metal-free nanoscale material in photocatalysis and electrocatalysis[J]. Rare Metals, 2024, 43: 3501-3552.

[6] Zhang H, Han X, Zhu J, et al. A metal-free boron carbon nitride (BCN) photocatalyst for enhanced CO_2-to-CH_4 conversion by surface electronic tuning[J]. Solar RRL, 2025: 202500037.

[7] Gao X, Li L, Zhao Z, et al. Sulfur vacancy-rich ZnS on ordered microporous carbon frameworks for efficient photocatalytic CO_2 reduction[J]. Applied Catalysis B: Environment and Energy, 2025, 364: 124835.

[8] Yang G, Xu Q, Zeng G. Developments of photo-/electro-catalysis based on covalent organic frameworks: a review[J]. Electron, 2024, 2: e39.

[9] Wang Y, Wu Y, Schwartz J, et al. A single-junction cathodic approach for stable unassisted solar water splitting[J]. Joule, 2019, 3: 2444-2456.

[10] Wang Y, Wu Y, Sun K, et al. A quadruple-band metal–nitride nanowire artificial photosynthesis system for high efficiency photocatalytic overall solar water splitting[J]. Materials Horizons, 2019, 6: 1454-1462.

[11] Xun W, Wang Y, Fan R, et al. Activating the MoS_2 basal plane toward enhanced solar hydrogen generation via in situ photoelectrochemical control[J]. ACS Energy Letters, 2021, 6: 267-276.

[12] Shen J, Wang Y, Chen C, et al. Reduced graphene oxide grafted on p-Si photocathode as a multifunctional interlayer for enhanced solar hydrogen production[J]. Applied Physics Letters, 2022, 121: 213901.

[13] Wang K, Huang D, Li X, et al. Unconventional strategies to break through the efficiency of light-driven water splitting: a review[J]. Electron, 2023, 1: e4.

[14] Inoue T, Fujishima A, Konishi S, et al. Photoelectrocatalytic reduction of carbon dioxide in aqueous suspensions of semiconductor powders[J]. Nature, 1979, 277: 637-638.

[15] Liu B, Ma L, Feng H, et al. Photovoltaic-powered electrochemical CO_2 reduction: benchmarking against the theoretical limit[J]. ACS Energy Letters, 2023, 8: 981-987.

[16] Gao X, Han X, Zhao Z, et al. Lewis functional nanodiamonds for efficient metal-free photocatalytic CO_2 reduction[J]. Journal of Materials Chemistry A, 2024, 12: 32745-32759.

[17] Wei P, Gao D, Liu T, et al. Coverage-driven selectivity switch from ethylene to acetate in high-rate CO_2/CO electrolysis[J]. Nature Nanotechnology, 2023, 18: 299-306.

[18] Yan Y, Wang H, Bi X, et al. Tandem catalysts CuSe/Au X for increasing local *CO concentration to promote the photocatalytic CO_2 reduction to C_2H_4[J]. Electron, 2023, 1: e3.

[19] Hoffmann M R, Martin S T, Choi W, et al. Environmental applications of semiconductor photocatalysis[J]. Chemical Reviews, 1995, 95: 69-96.

[20] Soni V, Singh P, Khan A A P, et al. Photocatalytic transition-metal-oxides-based p–n heterojunction materials: synthesis, sustainable energy and environmental applications, and perspectives[J]. Journal of Nanostructure in Chemistry, 2023, 13: 129-166.

[21] Mishra K, Devi N, Siwal S S, et al. Hybrid semiconductor photocatalyst nanomaterials for energy and environmental applications: fundamentals, designing, and prospects[J]. Advanced Sustainable Systems, 2023, 7: 2300095.

[22] Linsebigler A L, Lu G, Yates J T. Photocatalysis on TiO_2 surfaces: principles, mechanisms, and selected results[J]. Chemical Reviews, 1995, 95: 735-758.

[23] Xu T, Zhang L, Cheng H, et al. Significantly enhanced photocatalytic performance of ZnO via graphene hybridization and the mechanism study[J]. Applied Catalysis B: Environmental, 2011, 101: 382-387.

[24] Asahi R, Morikawa T, Ohwaki T, et al. Visible-light photocatalysis in nitrogen-doped titanium oxides[J]. Science, 2001, 293: 269-271.

[25] Li X, Chen Y, Tao Y, et al. Challenges of photocatalysis and their coping strategies[J]. Chem Catalysis, 2022, 2: 1315-1345.

[26] Ziwei Z, Xiaowu G, Wenxin C, et al. Research progress on the effects of surface functionalization of nanodiamonds[J]. Journal of Synthetic Crystals, 2022, 51: 852-864.

[27] Mochalin V N, Shenderova O, Ho D, et al. The properties and applications of nanodiamonds[J]. Nature Nanotechnology, 2012, 7: 11-23.

[28] Krüger A, Kataoka F, Ozawa M, et al. Unusually tight aggregation in detonation nanodiamond: identification and disintegration[J]. Carbon, 2005, 43: 1722-1730.

[29] Shenderova O, Koscheev A, Zaripov N, et al. Surface chemistry and properties of ozone-purified detonation nanodiamonds[J]. The Journal of Physical Chemistry C, 2011, 115: 9827-9837.

[30] Gibson N, Shenderova O, Luo T J M, et al. Colloidal stability of modified nanodiamond particles[J]. Diamond and Related Materials, 2009, 18: 620-626.

[31] Krueger A, Lang D. Functionality is key: recent progress in the surface modification of nanodiamond[J]. Advanced Functional Materials, 2012, 22: 890-906.

[32] Qin J X, Yang X G, Lv C F, et al. Nanodiamonds: synthesis, properties, and applications in nanomedicine[J]. Materials & Design, 2021, 210: 110091.

[33] Karami P, Salkhi Khasraghi S, Hashemi M, et al. Polymer/nanodiamond composites - a comprehensive review from synthesis and fabrication to properties and applications[J]. Advances in Colloid and Interface Science, 2019, 269: 122-151.

[34] Isberg J, Hammersberg J, Johansson E, et al. High carrier mobility in single-crystal plasma-deposited diamond[J]. Science, 2002, 297: 1670-1672.

[35] Zhang Y, Rhee K Y, Hui D, et al. A critical review of nanodiamond based nanocomposites: synthesis, properties and applications[J]. Composites Part B: Engineering, 2018, 143: 19-27.

[36] Hamers R J, Bandy J A, Zhu D, et al. Photoemission from diamond films and substrates into water: dynamics of solvated electrons and implications for diamond photoelectrochemistry[J]. Faraday Discuss., 2014, 172: 397-411.

[37] Zhang L, Zhu D, Nathanson G M, et al. Selective photoelectrochemical reduction of aqueous CO_2 to CO by solvated electrons[J]. Angewandte Chemie International Edition, 2014, 53: 9746-9750.

[38] Su L X, Huang Q Z, Lou Q, et al. Effective light scattering and charge separation in nanodiamond@g-C_3N_4 for enhanced visible-light hydrogen evolution[J]. Carbon, 2018, 139: 164-171.

[39] Ahmadijokani F, Molavi H, Bahi A, et al. Electrospun nanofibers of chitosan/polyvinyl alcohol/UiO-66/nanodiamond: versatile adsorbents for wastewater remediation and organic dye removal[J]. Chemical Engineering Journal, 2023, 457: 141176.

[40] Ahmadijokani F, Molavi H, Peyghambari A, et al. Efficient removal of heavy metal ions from aqueous media by unmodified and modified nanodiamonds[J]. Journal of Environmental Management, 2022, 316: 115214.

[41] Kim S H, Park S J. Interfacial interaction of graphitic carbon nitride/nanodiamond nanocomposites toward synergistic enhancement of photocatalytic degradation of organic contaminants[J]. Journal of Colloid and Interface Science, 2022, 608: 2257-2265.

[42] Molavi H, Mirzaei K, Jafarpour E, et al. Wastewater treatment using nanodiamond and related materials[J]. Journal of Environmental Management, 2024, 349: 119349.

[43] Tegafaw T, Liu S, Ahmad M Y, et al. Production, surface modification, physicochemical properties, biocompatibility, and bioimaging applications of nanodiamonds[J]. RSC Advances, 2023, 13: 32381-32397.

[44] Jain P G, Pathan A S, Jadhav Y S, et al. Nanodiamond: insight from introduction to application[J]. Current Nanoscience, 2023, 19: 817-824.

[45] Dolmatov V Yu, Ozerin A N, Kulakova I I, et al. Detonation nanodiamonds: new aspects in the theory and practice of synthesis, properties and applications[J]. Russian Chemical Reviews, 2020, 89: 1428-1462.

[46] Kira A, Tsutsumi Y, Tasaka A, et al. Generation of ultrahigh pressure and application of ultrahigh pressure to formation of diamond from graphite powder[J]. Materials Science Forum, 2011, 673: 275-278.

[47] Khan M B, Khan Z H. Nanomaterials and Their Applications[M]. Singapore: Springer Singapore, 2018: 1-26.

[48] Dolmatov V Y. Detonation-synthesis nanodiamonds: synthesis, structure, properties and applications[J]. Russian Chemical Reviews, 2007, 76: 339-360.

[49] Zou Q, Li Y G, Zou L H, et al. Characterization of structures and surface states of the nanodiamond synthesized by detonation[J]. Materials Characterization, 2009, 60: 1257-1262.

[50] Edgington R, Spillane K M, Papageorgiou G, et al. Functionalisation of detonation nanodiamond for monodispersed, soluble DNA-nanodiamond conjugates using mixed silane bead-assisted sonication disintegration[J]. Scientific Reports, 2018, 8: 728.

[51] Schrand A M, Hens S A C, Shenderova O A. Nanodiamond particles: properties and perspectives for bioapplications[J]. Critical Reviews in Solid State and Materials Sciences, 2009, 34: 18-74.

[52] Butler E, Hunt E, Fu Y P, et al. Investigating the governing decolorization mechanisms of nanodiamond in the treatment of an azo dye[J]. Desalination and Water Treatment, 2017, 86: 183-190.

[53] Hanada K. Detonation nanodiamond: perspective and applications[J]. Surface Engineering, 2009, 25: 487-489.

[54] Stehlik S, Varga M, Ledinsky M, et al. High-yield fabrication and properties of 1.4 nm nanodiamonds with narrow size distribution[J]. Scientific Reports, 2016, 6: 38419.

[55] Angus J C, Will H A, Stanko W S. Growth of diamond seed crystals by vapor deposition[J]. Journal of Applied Physics, 1968, 39: 2915-2922.

[56] Derjaguin B V, Fedoseev D V, Lukyanovich V M, et al. Filamentary diamond crystals[J]. Journal of Crystal Growth, 1968, 2: 380-384.

[57] Yang N, Yu S, Macpherson J V, et al. Conductive diamond: synthesis, properties, and electrochemical applications[J]. Chemical Society Reviews, 2019, 48: 157-204.

[58] Schwander M, Partes K. A review of diamond synthesis by CVD processes[J]. Diamond and Related Materials, 2011, 20: 1287-1301.

[59] Terranova M L, Rossi M, Tamburri E. Nanocrystalline sp^2 and sp^3 carbons: CVD synthesis and applications[J]. Crystallography Reports, 2016, 61: 897-906.

[60] Quan L. Research progress of CVD diamond film[J]. Chinese Journal of Vacuum Science and Technology, 2024, 44: 841-852.

[61] Fan L S, Constantin L, Li D wei, et al. Ultraviolet laser photolysis of hydrocarbons for nondiamond carbon suppression in chemical vapor deposition of diamond films[J]. Light: Science & Applications, 2017, 7: 17177-17177.

[62] Su Z K, Yuan S L, Li X L, et al. Prospects for ultrafast observation of femtosecond laser ablation in liquid(invited)[J]. Chinese Journal of Lasers, 2024, 51: 0402402.

[63] Pearce S R J, Henley S J, Claeyssens F, et al. Production of nanocrystalline diamond by laser ablation at the solid/liquid interface[J]. Diamond and Related Materials, 2004, 13: 661-665.

[64] Su J, Hu S L, Du X W. Carbon nanometer materials synthesized using laser ablation[J]. New Carbon Material, 2008, 23: 86-94.

[65] Zhao J X, Qiao Y L. Progress in preparation of carbon nanomaterials in liquid phase by pulsed laser ablation of graphite[J]. Materials Reports, 2017, 31: 32-37.

[66] Hao J, Li S, Dong M. Controllable preparation of bare nano-diamonds through femtosecond laser ablation in liquid[J]. Colloids and Surfaces A: Physicochemical and Engineering Aspects, 2025, 705: 135623.

[67] Frank F C, Lang A R, Moore M. Cavitation as a mechanism for the synthesis of natural diamonds[J]. Nature, 1973, 246: 143-144.

[68] Galimov E M. Possibility of natural diamond synthesis under conditions of cavitation, occurring in a fast-moving magmatic melt[J]. Nature, 1973, 243: 389-391.

[69] Galimov É M, Kudin A M, Skorobogatskii V N, et al. Experimental corroboration of the synthesis of diamond in the cavitation process[J]. Doklady Physics, 2004, 49: 150-153.

[70] Voropaev S A, Dnestrovskii A Yu, Skorobogatskii V N, et al. Experimental study into the formation of nanodiamonds and fullerenes during cavitation in an ethanol-aniline mixture[J]. Doklady Physics, 2014, 59: 503-506.

[71] Voropaev S. Cavitations synthesis of carbon nanostructures[J]. Journal of Physics: Conference Series, 2011, 291: 012028.

[72] Quinto-Su P A, Huang X H, Gonzalez-Avila S R, et al. Manipulation and microrheology of carbon nanotubes with laser-induced cavitation bubbles[J]. Physical Review Letters, 2010, 104: 014501.

[73] El-Eskandarany M S, Al-Hazza A, Al-Hajji L A, et al. Mechanical milling: a superior nanotechnological tool for fabrication of nanocrystalline and nanocomposite materials[J]. Nanomaterials, 2021, 11: 2484.

[74] Sharin P P, Sivtseva A V, Popov V I. Morphology and structural state of particles of nanopowders prepared by milling of natural diamond and by detonation synthesis[J]. Technical Physics Letters, 2020, 46: 145-149.

[75] El-Eskandarany M S. Mechanically induced graphite-nanodiamonds-phase transformations during high-energy ball milling[J]. Journal of Materials Engineering and Performance, 2017, 26: 2974-2982.

[76] Sumiya H, Harano K, Tamasaku K. HPHT synthesis and crystalline quality of large high-quality (001) and (111) diamond crystals[J]. Diamond and Related Materials, 2015, 58: 221-225.

[77] Dossa S S, Ponomarev I, Feigelson B N, et al. Analysis of the high-pressure high-temperature (HPHT) growth of single crystal diamond[J]. Journal of Crystal Growth, 2023, 609: 127150.

[78] Daulton T L, Kirk M A, Lewis R S, et al. Production of nanodiamonds by high-energy ion irradiation of graphite at room temperature[J]. Nuclear Instruments and Methods in Physics Research Section B: Beam Interactions with Materials and Atoms, 2001, 175-177: 12-20.

[79] Gogotsi Y, Welz S, Ersoy D A, et al. Conversion of silicon carbide to crystalline diamond-structured carbon at ambient pressure[J]. Nature, 2001, 411: 283-287.

[80] Kumar A, Ann Lin P, Xue A, et al. Formation of nanodiamonds at near-ambient conditions via microplasma dissociation of ethanol vapour[J]. Nature Communications, 2013, 4: 2618.

[81] Uwihoreye V, Hu Y, Cao G, et al. Recent progress on heteroepitaxial growth of single crystal diamond films[J]. Electron, 2024, 2: e70.

[82] Boudou J P, Tisler J, Reuter R, et al. Fluorescent nanodiamonds derived from HPHT with a size of less than 10nm[J]. Diamond and Related Materials, 2013, 37: 80-86.

[83] Christianson J R, Zhu D, Hamers R J, et al. Mechanism of N_2 reduction to NH_3 by aqueous solvated electrons[J]. The Journal of Physical Chemistry B, 2014, 118: 195-203.

[84] Zhu D, Zhang L, Ruther R E, et al. Photo-illuminated diamond as a solid-state source of solvated electrons in water for nitrogen reduction[J]. Nature Materials, 2013, 12: 836-841.

[85] Zhang L, Hamers R J. Photocatalytic reduction of CO_2 to CO by diamond nanoparticles[J]. Diamond and Related Materials, 2017, 78: 24-30.

[86] Roy N, Hirano Y, Kuriyama H, et al. Boron-doped diamond semiconductor electrodes: efficient photoelectrochemical CO_2 reduction through surface modification[J]. Scientific Reports, 2016, 6: 38010.

[87] O'Donnell K M, Edmonds M T, Tadich A, et al. Extremely high negative electron affinity of diamond via magnesium adsorption[J]. Physical Review B, 2015, 92: 035303.

[88] Takeuchi D, Kato H, Ri G S, et al. Direct observation of negative electron affinity in hydrogen-terminated diamond surfaces[J]. Applied Physics Letters, 2005, 86: 152103.

[89] Tiwari A K, Goss J P, Briddon P R, et al. Calculated electron affinity and stability of halogen-terminated diamond[J]. Physical Review B, 2011, 84: 245305.

[90] Beattie J M A. Electron-affinity and surface-stability of aluminium-oxide terminated diamond surfaces[J]. 2019, 94: 137-145.

[91] Yasu-eda T, Se-ike R, Ikenaga N oki, et al. Palladium-loaded oxidized diamond catalysis for the selective oxidation of alcohols[J]. Journal of Molecular Catalysis A: Chemical, 2009, 306: 136-142.

[92] Rietwyk K J, Wong S L, Cao L, et al. Work function and electron affinity of the fluorine-terminated (100) diamond surface[J]. Applied Physics Letters, 2013, 102: 091604.

[93] Pickett W E. Negative electron affinity and low work function surface: cesium on oxygenated diamond (100)[J]. Physical Review Letters, 1994, 73: 1664-1667.

[94] Nebel C E. Comprehensive Hard Materials[M]. Elsevier, 2014, 3: 339-364.

[95] Miliaieva D, Djoumessi A S, Čermák J, et al. Absolute energy levels in nanodiamonds of different origins and surface chemistries[J]. Nanoscale Advances, 2023, 5: 4402-4414.

[96] Abel B, Buck U, Sobolewski A L, et al. On the nature and signatures of the solvated electron in water[J]. Phys. Chem. Chem. Phys., 2012, 14: 22-34.

[97] Herbert J M, Coons M P. The hydrated electron[J]. Annual Review of Physical Chemistry, 2017, 68: 447-472.

[98] Liu G, Feng C, Shao P. Degradation of perfluorooctanoic acid with hydrated electron by a heterogeneous catalytic system[J]. Environmental Science & Technology, 2022, 56: 6223-6231.

[99] Gu L X, Yang K, Teng Y, et al. Diamond-based electron emission: Structure, properties and mechanisms[J]. Chinese Physics B, 2024, 33: 098102.

[100] Sagar D M, Bain Colin D, Verlet J R R. Hydrated electrons at the water/air interface[J]. Journal of the American Chemical Society, 2010, 132: 6917-6919.

[101] Buchner F, Kirschbaum T, Venerosy A, et al. Early dynamics of the emission of solvated electrons from nanodiamonds in water[J]. Nanoscale, 2022, 14: 17188-17195.

[102] Maza W A. Degradation of perfluorooctanesulfonate (PFOS) by sub-bandgap irradiation of hydrogen-terminated nanodiamond[J]. 2023, 325: 122306.

[103] Jang D M, Myung Y, Im H S, et al. Nanodiamonds as photocatalysts for reduction of water and graphene oxide[J]. Chem. Commun., 2012, 48: 696-698.

[104] Zhu D, Bandy J A, Li S, et al. Amino-terminated diamond surfaces: photoelectron emission and photocatalytic properties[J]. Surface Science, 2016, 650: 295-301.

[105] Khan M, Hayat A, Baburao Mane S K, et al. Functionalized nano diamond composites for photocatalytic hydrogen evolution and effective pollutant degradation[J]. International Journal of Hydrogen Energy, 2020, 45: 29070-29081.

[106] Catone D, Di Mario L, Martelli F, et al. Ultrafast optical spectroscopy of semiconducting and plasmonic nanostructures and their hybrids[J]. Nanotechnology, 2020, 32: 025703.

[107] Linic S, Aslam U, Boerigter C, et al. Photochemical transformations on plasmonic metal nanoparticles[J]. Nature Materials, 2015, 14: 567-576.

[108] Ninakanti R, Dingenen F, Borah R, et al. Plasmonic hybrid nanostructures in photocatalysis: structures, mechanisms, and applications[J]. Topics in Current Chemistry, 2022, 380: 40.

[109] Ma J, Zhang X, Gao S. Tunable electron and hole injection channels at plasmonic Al–TiO_2 interfaces[J]. Nanoscale, 2021, 13: 14073-14080.

[110] Wu N. Plasmonic metal–semiconductor photocatalysts and photoelectrochemical cells: a review[J]. Nanoscale, 2018, 10: 2679-2696.

[111] Cushing S K, Bristow A D, Wu N. Theoretical maximum efficiency of solar energy conversion in plasmonic metal–semiconductor heterojunctions[J]. Physical Chemistry Chemical Physics, 2015, 17: 30013-30022.

[112] Bellucci A, Campanari V, Mastellone M, et al. Optical characteristics of nanostructured aluminium/diamond composite systems in the visible range[J]. Diamond and Related Materials, 2023, 132: 109669.

[113] Huang F, Peng M, Liu H, et al. Atomically dispersed metals on nanodiamond-derived hybrid materials for heterogeneous catalysis[J]. Accounts of Materials Research, 2023, 4: 223-236.

[114] Yadav M, Gyulavári T, Kiss J, et al. Noble metal nanoparticles and nanodiamond modified strontium titanate photocatalysts for room temperature CO production from direct hydrogenation of CO_2[J]. Journal of CO_2 Utilization, 2023, 78: 102621.

[115] Orlanducci S, Ammirati G, Bellucci A, et al. Gold-diamond nanocomposites efficiently generate hydrated electrons upon absorption of visible light[J]. ACS Applied Optical Materials, 2024, 2: 1180-1187.

[116] Li S, Bandy J A, Hamers R J. Enhanced photocatalytic activity of diamond thin films using embedded Ag nanoparticles[J]. ACS Applied Materials & Interfaces, 2018, 10: 5395-5403.

[117] Wang Z, Zhang F, Ning A, et al. Nanosilver supported on inert nano-diamond as a direct plasmonic photocatalyst for degradation of methyl blue[J]. Journal of Environmental Chemical Engineering, 2021, 9: 104912.

[118] Manickam-Periyaraman P, Espinosa S M, Espinosa J C, et al. Dyes decolorization using silver nanoparticles supported on nanometric diamond as highly efficient photocatalyst under natural sunlight irradiation[J]. Journal of Environmental Chemical Engineering, 2016, 4: 4485-4493.

[119] Honda M, Ochiai T, Listiani P, et al. Low-temperature synthesis of Cu-doped anatase TiO_2 nanostructures via liquid phase deposition method for enhanced photocatalysis[J]. Materials, 2023, 16: 639.

[120] Sirivallop A, Areerob T, Chiarakorn S. Enhanced visible light photocatalytic activity of N and Ag doped and co-doped TiO_2 synthesized by using an in-situ solvothermal method for gas phase ammonia removal[J]. Catalysts, 2020, 10: 251.

[121] Zhang J, Li J. The oxygen vacancy defect of ZnO/NiO nanomaterials improves photocatalytic performance and ammonia sensing performance[J]. Nanomaterials, 2022, 12: 433.

[122] Elfimchev S, Chandran M, Akhvlediani R, et al. Visible sub-band gap photoelectron emission from nitrogen doped and undoped polycrystalline diamond films[J]. Applied Surface Science, 2017, 410: 414-422.

[123] Su R, Liu Z, Abbasi H N, et al. Visible-light activation of photocatalytic for reduction of nitrogen to ammonia by introducing impurity defect levels into nanocrystalline diamond[J]. Materials, 2020, 13: 4559.

[124] Yoshikawa T, Asakawa H, Matsumoto T, et al. CO_2 reduction by visible-light-induced photoemission from heavily N-doped diamond nano-layer[J]. Carbon, 2024, 218: 118689.

[125] Hunge Y M, Yadav A A, Khan S, et al. Photocatalytic degradation of bisphenol A using titanium dioxide@nanodiamond composites under UV light illumination[J]. Journal of Colloid and Interface Science, 2021, 582: 1058-1066.

[126] Liu J, Wang P, Qu W, et al. Nanodiamond-decorated ZnO catalysts with enhanced photocorrosion-resistance for photocatalytic degradation of gaseous toluene[J]. Applied Catalysis B: Environmental, 2019, 257: 117880.

[127] Kublik N, Gomes L E, Plaça L F, et al. Metal-free g-C_3N_4/nanodiamond heterostructures for enhanced photocatalytic pollutant removal and bacteria photoinactivation[J]. Photochem, 2021, 1: 302-318.

[128] Kim H, Kim H na, Weon S, et al. Robust co-catalytic performance of nanodiamonds loaded on WO_3 for the decomposition of volatile organic compounds under visible light[J]. ACS Catalysis, 2016, 6: 8350-8360.

[129] Lin Z, Xiao J, Li L, et al. Nanodiamond-embedded p-type copper(I) oxide nanocrystals for broad-spectrum photocatalytic hydrogen evolution[J]. Advanced Energy Materials, 2016, 6: 1501865.

[130] Geis M W, Efremow N N, Krohn K E, et al. A new surface electron-emission mechanism in diamond cathodes[J]. Nature, 1998, 393: 431-435.

[131] Xu X, Guo Z, Wei J, et al. Highly efficient defluorination of perfluorooctanoic acid by a BiOCl-ND photocatalyst: enhanced charge transfer and synergistic mechanism[J]. Journal of Cleaner Production, 2024, 475: 143629.

[132] Henych J, Stehlík Š, Mazanec K, et al. Reactive adsorption and photodegradation of soman and dimethyl methylphosphonate on TiO_2/nanodiamond composites[J]. Applied Catalysis B: Environmental, 2019, 259: 118097.

[133] Sagara N, Kamimura S, Tsubota T, et al. Photoelectrochemical CO_2 reduction by a p-type boron-doped g-C_3N_4 electrode under visible light[J]. Applied Catalysis B: Environmental, 2016, 192: 193-198.

[134] Wen J, Xie J, Chen X, et al. A review on g-C_3N_4-based photocatalysts[J]. Applied Surface Science, 2017, 391: 72-123.

[135] Zhou L, Zhang H, Guo X, et al. Metal-free hybrids of graphitic carbon nitride and nanodiamonds for photoelectrochemical and photocatalytic applications[J]. Journal of Colloid and Interface Science, 2017, 493: 275-280.

[136] Lin Y, Sun X, Su D S, et al. Catalysis by hybrid sp^2/sp^3 nanodiamonds and their role in the design of advanced nanocarbon materials[J]. Chemical Society Reviews, 2018, 47: 8438-8473.

[137] Haleem Y A. Facile synthesis of mesoporous detonation nanodiamond-modified layers of graphitic carbon nitride as photocatalysts for the hydrogen evolution reaction[J]. RSC Advances, 2017, 7: 15390-15396.

[138] Su L X, Liu Z Y, Ye Y L, et al. Heterostructured boron doped nanodiamonds@g-C_3N_4 nanocomposites with enhanced photocatalytic capability under visible light irradiation[J]. International Journal of Hydrogen Energy, 2019, 44: 19805-19815.

[139] Su L X, Lou Q, Shan C X, et al. Ag/Nanodiamond/g-C_3N_4 heterostructures with enhanced visible-light photocatalytic performance[J]. Applied Surface Science, 2020, 525: 146576.

[140] Su L X, Lou Q, Shan C X, et al. A novel MoS_2-modified hybrid nanodiamond/g-C_3N_4 photocatalyst for photocatalytic hydrogen evolution[J]. Chemical Physics, 2024, 577: 112135.

[141] Li X, Li S, Xu J, et al. Synergy of nitrogen vacancies and nanodiamond decoration in g-C_3N_4 for boosting CO_2 photoreduction[J]. Applied Surface Science, 2022, 600: 154199.